Annals of Operations Research
https://doi.org/10.1007/s10479-026-07397-2

ORIGINAL RESEARCH

A sustainability-aware optimization framework for port-hinterland truck scheduling

Ali Mokhtari-Moghadam[1] · Trung Thanh Nguyen[1] · Massoud Mohsendokht[1] · Jin Wang[1] · Zaili Yang[1]

Received: 13 February 2026 / Accepted: 14 August 2026

Abstract
Ports are critical gateways for trade and regional growth but also generate substantial externalities such as emissions, congestion, and safety risks. Growing maritime transport and port throughput intensify long-haul diesel truck traffic on hinterland access roads, causing peak-hour bottlenecks, long queues, and higher environmental impacts. Despite many proposed operational strategies, these challenges remain insufficiently addressed. This paper develops a mixed-integer linear programming (MILP) model for sustainable port-hinterland truck scheduling within an integrated chassis-based remote gate (CRG) and battery-electric trucks (BET) framework for short-haul transport. Using a major UK port case study with real traffic data, the model minimizes total logistics costs, including fixed investments, transport, waiting and idling times for short- and long-haul trucks, and CO_2 emissions. To handle large-scale instances, a two-stage adaptive genetic algorithm (TS-AGA) is proposed and benchmarked against the MILP and a two-stage simulated annealing approach. Collaborative and non-collaborative scheduling strategies are compared to assess the benefits of coordinated decision-making. Results show that collaborative scheduling reduces total system costs by about 13.6% by better synchronizing long-haul diesel truck arrivals with short-haul battery-electric truck operations. Sensitivity analysis further examines how long-haul travel-time uncertainty affects congestion and economic performance. Overall, the proposed MILP model and TS-AGA solution approach demonstrate that coordinated truck scheduling can substantially improve the operational efficiency and sustainability of CRG-BET-based port-hinterland systems. By jointly optimizing long-haul and short-haul operations under collaborative and uncertainty-aware strategies, the study offers a practical

✉ Trung Thanh Nguyen
T.T.Nguyen@ljmu.ac.uk

Ali Mokhtari-Moghadam
A.MokhtariMoghadam@2024.ljmu.ac.uk

Massoud Mohsendokht
M.Mohsendokhtamlashi@ljmu.ac.uk

Jin Wang
J.Wang@ljmu.ac.uk

Zaili Yang
Z.Yang@ljmu.ac.uk

[1] School of Engineering and Built Environment, Liverpool John Moores University, Liverpool, UK

Published online: 09 September 2026

and scalable scheduling methodology to reduce logistics costs, congestion, and emissions while supporting sustainable port-city connectivity.

Keywords Port-city logistics · Port congestion · Emission · Remote gate · Optimization · Truck scheduling

1 Introduction

Ports serve as key economic hubs by connecting maritime shipping with inland transportation networks (Aregall et al., 2018). Within transport and logistics systems, port-hinterland transport contributes significantly to negative externalities, including greenhouse gas (GHG) emissions, air pollution, traffic congestion, and accidents. Despite these challenges, road transport remains the dominant mode for hinterland freight movements, even though it performs poorly in terms of environmental sustainability (Guo et al., 2023). From a cost perspective, inland operations account for 40–80% of total container transport expenses (Notteboom and Rodrigue, 2005). With the advent of larger vessels and increasing economies of scale in maritime shipping, these inland transport costs often exceed maritime transport costs (Bouchery et al., 2020).

The negative externalities associated with port-hinterland operations are further exacerbated when ports are located within or near urban areas, commonly referred to as port cities (Schulte et al., 2017). In such settings, opportunities for physical expansion are often limited despite growing throughput demands due to land scarcity. Furthermore, existing road infrastructure is frequently unable to accommodate the high volume of truck traffic, particularly during peak periods. As a result, access roads to and from port cities often become congested, disrupting the efficient pickup and delivery of containers. This can undermine the operational performance of the port-hinterland system and intensify traffic congestion and emissions in surrounding areas, attracting increasing attention from both the public and government authorities.

Over the past two decades, numerous operational strategies have been proposed to mitigate port congestion and improve terminal performance. These include truck appointment systems, collaborative truck scheduling, yard automation, chassis exchange terminals, and infrastructure expansion. Although these approaches have improved gate operations and reduced truck turnaround times, they primarily optimize activities within the port boundary and pay limited attention to congestion, emissions, and traffic generated by diesel trucks traveling through surrounding urban areas. Consequently, many emerging port-city logistics challenges remain insufficiently addressed.

Inland facilities such as extended gates, inland terminals, and dry ports have emerged as alternative solutions to these challenges, supporting sustainable port-hinterland connectivity, particularly in port cities, by shifting a significant share or even the entirety of short- and long-haul container movements from road to rail (Roso et al., 2009). However, road transport nevertheless remains the dominant mode, accounting for approximately 78% of total hinterland freight transport (Uic, 2024). Consequently, optimization approaches that rely primarily on modal shift are less applicable in regions where road transport remains the dominant freight mode. This highlights the need for sustainable road-based logistics solutions that improve port-city connectivity without requiring major rail infrastructure investment.

To address the limitations of conventional inland terminals in road-dominated freight networks, Mokhtari-Moghadam et al. (2025) proposed the integrated chassis-based remote gate with battery-electric trucks (CRG-BET), a network-oriented framework that relocates long-haul diesel trucks to a remote gate outside the urban area while employing battery-electric trucks for short-haul container transport between the remote gate and the seaport. Compared with rail-based dry ports, the framework requires lower infrastructure investment and better exploits existing road networks while substantially reducing emissions, congestion, and truck turnaround times.

Despite its promising performance, the CRG-BET framework leaves several important operational challenges unresolved. First, long-haul truck arrivals are treated as exogenous and follow temporal patterns similar to those observed in conventional systems, rather than being integrated into an optimized scheduling framework. Second, the interaction between long-haul internal combustion engine (ICE) truck arrivals and short-haul battery-electric truck operations requires coordinated scheduling decisions to effectively balance port and remote-gate operations, which has not yet been investigated. Third, previous studies assume fixed handling capacities at both the seaport and the remote gate, overlooking substantial temporal variations caused by quay-side operational priorities and unexpected disruptions. Consequently, the operational potential of the CRG-BET framework under realistic and dynamic port conditions remains largely unexplored.

To address these limitations, this paper develops a sustainability-aware optimization framework for the port-hinterland truck scheduling problem (PHTSP). Unlike previous studies, the proposed framework jointly optimizes long-haul ICE truck scheduling and battery-electric shuttle truck operations and evaluates the impacts of collaborative and non-collaborative scheduling strategies under time-varying handling capacities at both the port and the remote gate. A MILP model is formulated to determine optimal scheduling decisions while evaluating the operational and economic performance of the CRG-BET system in terms of logistics costs, congestion, and emissions. To solve large-scale real-world instances, the MILP model is complemented by a tailored TS-AGA, and sensitivity analyses are conducted to investigate the impacts of travel-time uncertainty on system performance.

The main contributions of this research are as follows:

(1) Integrated truck scheduling optimization framework: This study develops an optimization framework for CRG-BET-based port-hinterland logistics that jointly determines long-haul ICE truck schedules and battery-electric shuttle truck operations. Unlike existing truck scheduling and remote-gate studies, the proposed framework integrates port, remote-gate, and hinterland operations within a unified scheduling model.

(2) Realistic operational modeling of port-city logistics: A sustainability-aware MILP model is formulated for the PHTSP by incorporating real-world operational characteristics, including time-varying handling capacities at the seaport and remote gate and observed long-haul truck arrival patterns. The model minimizes the total system cost, which integrates transportation, operational, queuing, parking, emission, land rental, and chassis hiring costs.

(3) Scalable optimization methodology: A problem-specific TS-AGA is developed that hierarchically optimizes fleet composition and truck scheduling using customized chromosome encoding, adaptive search operators, and problem-specific feasibility evaluation, enabling efficient solution of large-scale PHTSP instances beyond the practical capability of exact optimization.

(4) Evaluation of coordinated scheduling and uncertainty impacts: The proposed framework evaluates the benefits of coordinated scheduling compared with independent truck operations and investigates the influence of long-haul travel-time deviations on logistics costs, truck waiting and idling times, congestion, and emissions within the port-CRG-hinterland system.

(5) Managerial and policy insights: The findings provide practical recommendations for port authorities, logistics operators, and policymakers regarding the implementation of CRG-BET systems and coordinated scheduling strategies to improve port-city connectivity, reduce freight-related externalities, and enhance sustainable logistics performance.

The remainder of this study is structured as follows: Section 2 reviews the relevant literature and identifies the research gaps. Section 3 describes the problem and presents the mathematical formulation. Section 4 details the proposed evolutionary algorithm. Section 5 presents the computational results and analysis, including sensitivity analyses and managerial insights. Finally, Section 6 concludes the paper with final remarks and future research directions.

2 Related work and research gaps

This section reviews the existing literature on sustainable port-hinterland logistics, focusing on three main research streams: (i) network-oriented strategies for improving port-city connectivity, including inland terminals, dry ports, and remote gate concepts; (ii) truck scheduling and collaboration strategies for mitigating port congestion and reducing transport-related externalities; and (iii) optimization approaches for improving the operational efficiency and sustainability of port-hinterland systems. Based on this review, the key research gaps motivating the proposed CRG-BET-based port-hinterland truck scheduling optimization framework are identified.

2.1 Port-city freight transport and hinterland connectivity

In recent decades, inland intermodal terminals have become increasingly important for alleviating congestion at seaports while improving port-hinterland connectivity. In this study, the term *inland intermodal terminal* is used broadly to encompass a range of land-based facilities discussed in the literature, including dry ports, inland ports, satellite terminals, extended gates, and other inland logistics nodes whose specific roles and spatial configurations vary across applications. Fundamentally, these facilities act as connection points within intermodal transport systems, enabling the sequential use of multiple transport modes, most commonly road-rail, road-waterway, and road-rail-road combinations (Dong et al., 2020).

Although the dry port concept originated in a report by Unctad (1982) and was subsequently implemented in practice (Rodrigue et al., 2010; Roso et al., 2009), its theoretical development and systematic investigation have largely emerged over the past two decades. Roso (2007) evaluated the feasibility of dry ports from an environmental perspective, estimating that implementing a dry port could reduce CO_2 emissions by 25% while significantly decreasing truck waiting times and port congestion. Roso et al. (2009) further introduced the dry port concept as a sustainable strategy to enhance port-hinterland connectivity, emphasizing the use of high-capacity transport modes such as rail to link inland dry ports with seaports and thereby alleviate congestion in port cities. The important role of inland terminals in port-hinterland logistics was also explored by Rodrigue and Notteboom (2009). Later, Rodrigue et al. (2010) defined inland ports as intermodal logistics hubs primarily engaged in container handling and value-added logistics activities, connected to seaports through high-capacity transport corridors, preferably by rail or barge. Such integration supports economies of scale in inland distribution while improving the efficiency of port-hinterland freight transport.

The integration of supply chains and transport networks through the extension of seaport terminal operations to inland locations was examined by Veenstra et al. (2012), who discussed the relationship between the extended gate and dry port concepts. They emphasized that properly implemented extended gates can foster modal shift, enhance logistics efficiency, and promote regional development. Beyond their traditional role as hinterland extensions of seaports, Wiegmans et al. (2020) argued that inland ports are increasingly evolving into strategic logistics hubs that proactively influence freight flows and regional hinterland development. The effectiveness of inland terminals also depends on the transport modes used to connect them with seaports. For example, Afiatno et al. (2025) evaluated truck, rail, and barge transport for container movements via dry ports using a multi-criteria framework considering transportation cost, transit time, and intermodal connectivity. Their results indicate that the preferred transport mode depends on shipment size, with barges offering the lowest cost for single-TEU shipments, trucks remaining competitive for smaller volumes, and rail providing the shortest transit times.

While most studies have focused on rail- or barge-based inland terminals, Mokhtari-Moghadam et al. (2025) proposed an alternative approach to improving sustainable port-city connectivity based on unimodal road transport, which is particularly suitable for countries with road-dominated freight logistics networks. Their network-oriented framework introduces a CRG located on the outskirts of the city, where long-haul ICE trucks arriving from inland nodes, including inland terminals, are redirected to the CRG rather than entering the seaport. Battery electric trucks are then deployed to transport containers between the seaport and the CRG. Using a systematic analysis, the authors examined how the balance and imbalance between port and hinterland truck-handling capacities affect key performance metrics, including total cost, CO_2 emissions, port congestion, congestion on port-access roads, and traffic density. Their findings highlight the importance of coordinated port-hinterland connectivity, demonstrating that the proposed CRG-BET framework outperforms the conventional system by reducing negative externalities at the port and along port-access roads while also lowering total costs under port and hinterland capacity constraints.

2.2 Collaborative and sustainable truck scheduling

Unlike network-oriented strategies that aim to alleviate port gate congestion and enhance sustainable port-hinterland connectivity by reducing the negative externalities associated with ICE trucks, another stream of research focuses on the seaport as the primary bottleneck and investigates operational strategies to improve terminal efficiency. This line of research mainly addresses congestion arising from uncertain external truck arrivals, particularly during peak periods.

To improve truck flow management and mitigate gate congestion, several ports, most notably the Ports of Los Angeles and Long Beach, were among the first to implement truck appointment systems (TAS). TAS aims to distribute truck arrivals more evenly by shifting peak-time demand to off-peak periods while considering yard capacity constraints. Effective management of truck arrivals can reduce truck turnaround time (TTT) and consequently improve container terminal performance (Huynh et al., 2005). Guan et al. (2009) highlighted the importance of TAS and its benefits for multiple stakeholders by developing a multi-server queuing model to analyse port congestion and truck waiting-time costs. Beyond reducing gate congestion, Zhao and Goodchild (2010) and van Asperen et al. (2013) investigated the role of advance information on truck arrival times in minimizing container rehandling operations within the yard and improving the efficiency of yard crane operations.

Although TAS provides benefits for both port authorities and trucking companies (TCs), mandatory appointment systems may not always be attractive to TCs, as they can reduce truck utilization and increase operational costs (Azab et al., 2020). To improve stakeholder participation, Phan and Kim (2015) proposed a negotiation framework between TCs and container terminals to determine mutually acceptable truck arrival windows, thereby minimizing deviations from preferred schedules and reducing gate waiting times. To further improve the estimation of truck waiting times and TTT, (Azab et al., 2020) developed a simulation-based optimization model.

In addition to congestion reduction, recent studies have extended TAS to address broader operational objectives. Caballini et al. (2020) proposed a clustering-based approach to match import and export containers, thereby reducing empty truck movements while minimizing deviations between truck schedules and designated appointment windows. Similarly, da Silva et al. (2023) developed a flexible TAS using a machine learning and simulation-based approach that enables dynamic rescheduling of truck appointments based on predicted gate waiting times. Their approach uses real-time truck location data and checkpoint information to estimate travel times, predict queueing delays, and dynamically adjust appointment schedules accordingly. Furthermore, Schulte et al. (2017) extended the conventional role of TAS, which traditionally focuses on congestion mitigation and TTT reduction, by incorporating collaborative mechanisms among trucking companies. They developed a graph-based mathematical model that enables carriers to coordinate trips, share transportation capacity, and schedule corresponding appointments through TAS, with the objective of reducing empty truck movements, emissions, and overall operational costs.

Despite these advances, TAS-based approaches primarily focus on managing truck arrivals at the port gate and improving terminal-side operations. They generally do not consider the integrated scheduling of truck movements across the wider port-hinterland system, particularly the coordination between long-haul freight movements and short-haul transport operations outside the port boundary.

Beyond appointment-based approaches, Dekker et al. (2013) introduced chassis exchange terminals (CETs) as an alternative strategy for mitigating port gate congestion by relocating container exchanges from the port to nearby inland facilities. Containers are subsequently transported to the port during off-peak periods, thereby reducing pressure on port gate operations.

2.3 Optimization and simulation approaches for sustainable port-hinterland operations

Optimization- and simulation-based approaches have been widely applied to improve the efficiency and sustainability of port-hinterland logistics, including inland terminal planning, intermodal network design, and truck scheduling decisions.

Sciomachen and Stecca (2023) analyzed the effects of container arrival rates on port-related networks and proposed a MILP model to optimize container forwarding to dry ports. Their model accounts for network capacity and time-dependent travel costs, aiming to reduce congestion and improve container flow management. Similarly, Tsao and Thuy (2018) developed a continuous approximation model for seaport-dry port network design with multi-modal transport (road and rail), incorporating game theory and nonlinear optimization to minimize carbon costs. Their results indicate that shippers located near seaports prefer direct routes, while those farther away favor dry ports. Large nations derive the greatest economic benefits, whereas rail-developed countries experience environmental advantages. However, higher carbon and holding costs were shown to reduce profits, underscoring the need for greener, rail-based dry port operations.

Lättilä et al. (2013) developed a discrete-event simulation model to evaluate the feasibility of implementing dry ports in Finland by analyzing CO_2 emissions and transportation costs. Their results indicate that the use of dry ports can reduce emissions by up to 45% and transportation costs by 4–16%. Benedecti et al. (2024) proposed an inland container terminal and waterway service between Joinville and Itapoá Port, evaluated through agent-based simulation and financial analysis. Their findings demonstrate both operational and economic viability, showing a 2% reduction in end-customer costs, a 65% decrease in truck dwell time, and a 65% cut in greenhouse gas emissions. These benefits stem from a 49% reduction in the number of trucks and an 84% decrease in travel distance.

While many optimization studies focus on network design and modal selection (Bagheri et al., 2025; Facchini et al., 2020; Irawan et al., 2024; Kurtuluş, 2022; Raad et al., 2022), operational truck scheduling has also been explored to improve the efficiency of port-hinterland transport operations. For example, Zhen et al. (2022) developed a truck scheduling decision support system (DSS) to minimize the operational costs of the Yongfeng Trucking Company by optimizing truck movements between the port yard and hinterland. They formulated a MILP model and proposed a heuristic algorithm to obtain high-quality solutions for a real-world case study within reasonable computational time. Their findings demonstrate that the proposed DSS can reduce total logistics costs by approximately 22% while improving customer satisfaction.

In parallel with centralized optimization approaches, game-theoretic models have been applied in sustainable maritime transportation to capture strategic interactions among multiple stakeholders, particularly in environmental management and policy-related decision-making (Zhuge et al., 2024). These approaches generally consider decentralized decision-making among stakeholders with potentially conflicting objectives. However, they are less suitable for collaborative planning among interconnected actors within a port-hinterland logistics system, where coordinated decisions need to be jointly optimized to improve system-wide performance. In such contexts, centralized optimization frameworks, such as MILP, provide an appropriate approach for determining coordinated decisions while accounting for operational constraints and system-wide cost objectives.

Despite advances in truck scheduling optimization, existing studies mainly focus on conventional port-hinterland operations and rarely consider the integration of remote-gate systems, battery-electric truck operations, or the coordination of truck schedules under time-varying port and inland handling capacities.

2.4 Research gaps and motivation

A review of the existing literature reveals several key research gaps:

(1) Existing truck scheduling approaches, including TAS-based optimization and CET strategies, primarily focus on mitigating congestion within or near the port boundary. Although these approaches improve gate operations and truck turnaround times, they generally overlook the wider port-hinterland logistics system, particularly the congestion and emissions generated by diesel trucks traveling through urban port-access corridors. Consequently, their ability to address emerging port-city logistics challenges remains limited.

(2) Optimization studies based on inland intermodal terminals mainly rely on modal shift towards rail or waterway transport. However, road transport remains the dominant freight mode in many regions due to infrastructure limitations and geographical constraints. Therefore, there is a need for sustainable road-based solutions that improve port-city connectivity without requiring extensive investment in new rail infrastructure.

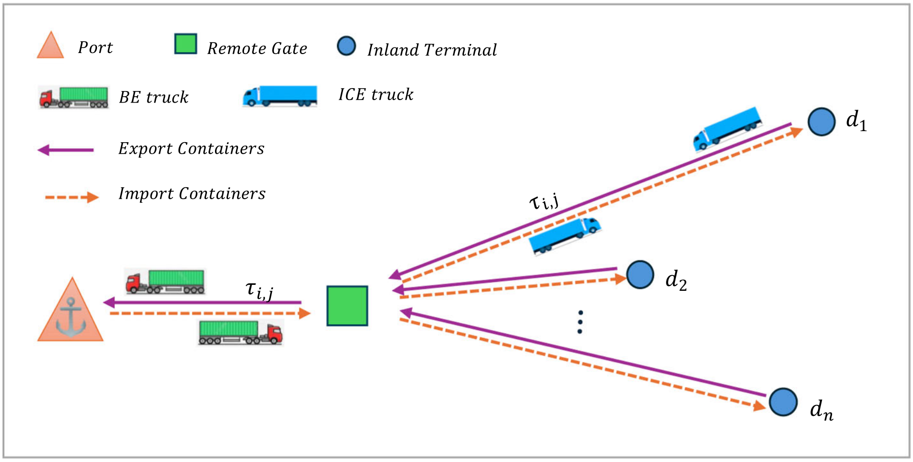

Fig. 1 Illustration of the two-layer CRG-BET port-hinterland truck scheduling framework based on theconcept introduced by Mokhtari-Moghadam et al. (2025)

(3) Although studies on the CRG-BET framework remain limited, they demonstrate its potential as a sustainable alternative for improving port-city connectivity. However, several operational challenges remain unresolved. Existing studies assume that long-haul ICE truck arrivals follow predefined temporal patterns similar to conventional systems rather than being determined through an integrated scheduling framework. Moreover, the joint scheduling of long-haul ICE truck arrivals and short-haul battery-electric truck operations has not been investigated. Furthermore, previous studies assume fixed handling capacities at both the port and CRG, overlooking temporal variations caused by quay-side operational priorities and unexpected disruptions. These limitations restrict the evaluation of CRG-BET performance under realistic and dynamic operating conditions.

3 Problem description and mathematical formulation

3.1 Problem description

This section describes the operational structure of the CRG-BET system and formulates the associated PHTSP. As illustrated in Fig. 1, the system consists of two interconnected operational layers: (i) long-haul container transportation between inland terminals and the remote gate, and (ii) short-haul container transfer between the remote gate and the seaport using battery-electric trucks.

There is a set of inland terminals, $D = 1, 2, \ldots, d_n$, each located at a different site and serving as a consolidation and distribution hub for long-haul container flows associated with exporters (shippers) and importers (consignees). Each inland terminal handles export containers originating from shippers with quantity q'_d and import containers destined for consignees with quantity q_d. A fleet of ICE trucks, $V = 1, 2, \ldots, |V|$ transports export-loaded containers from inland terminals to the CRG, denoted by r. After delivering an export-loaded chassis at the CRG, an ICE truck typically returns to its originating inland terminal with the first available import-loaded chassis. The transfer of containers between the CRG and the seaport is performed by a fleet of BE trucks, $K = 1, 2, \ldots, |K|$. Each BE truck

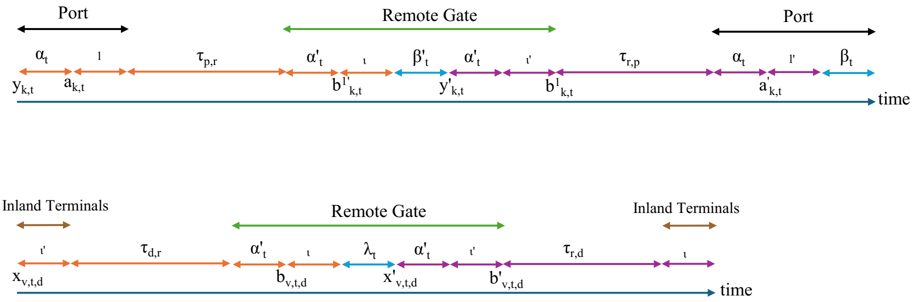

Fig. 2 Illustration of truck status in time

$k \in K$ collects an import-loaded chassis at the seaport and transports it to the CRG, where it decouples the chassis in the designated import area before coupling an export-loaded chassis for the return trip to the port. Upon arriving at the seaport, the BE truck proceeds to the stacking yard, where the export container is unloaded and a new import container is loaded onto the same chassis without decoupling it. The truck then returns to the CRG with the newly loaded import container, thereby completing one operating cycle. Fig. 2 illustrates the evolution of the truck operating states over time.

The model considers the scheduling of both truck fleets under time-varying facility capacities at the port and the remote gate over the planning horizon. The primary objective is to minimize total system cost, including transportation costs, operating costs of trucks, chassis hiring costs, truck queuing costs, parking costs associated with truck idle times awaiting new assignments, land-use costs at the remote gate for accommodating chassis, and CO_2 emission costs generated by trucks during queuing periods.

The main assumptions underlying the proposed model are summarized as follows:

(1) The ICE and BE truck fleets are operated by separate logistics operators. In the non-collaborative scenario, each fleet follows its own operational schedule based on conventional truck arrival patterns. In the collaborative scheduling scenario, operational information is shared among relevant stakeholders, and ICE and BE truck movements are coordinated according to the optimized schedules generated by the proposed framework. For example, an ICE truck arriving at the CRG from d_1 is not required to wait for a return container associated with the same inland terminal; instead, it can be assigned the first available compatible import container, thereby reducing idle time and improving fleet utilization.
(2) The CRG is operated by the port authority. Its objective is to improve the overall performance of the port-hinterland system by reducing congestion, emissions, and operational costs while optimizing CRG resources, including chassis requirements and facility utilization.
(3) The planning horizon is defined as a single operational day (24 h), during which all import and export container demands must be satisfied.
(4) The handling capacities of both the seaport and the CRG are time-varying and assumed to be known in advance based on available operational information.
(5) Each truck can transport only one chassis per trip.

Table 1 Indices and parameters for the model

Notation	Definition
Indices	
i, j	Indices of nodes within the network
d	Index of inland terminals, $d \in \{1, 2, \ldots, D\}$
p	Index of port
r	Index of remote gate (CRG)
t	Index of discrete time slots, $t \in \{1, 2, \ldots, T\}$, each of length $\Delta = 10$ minutes
h	Index of hours, $h \in \{1, 2, \ldots, H\}$
v	Index of ICE trucks (inland terminals $\leftrightarrow$ remote gate), $v \in \{1, \ldots, V\}$
k	Index of BE trucks (port $\leftrightarrow$ remote gate), $k \in \{1, \ldots, K\}$
Parameters	
q_d	Containers to be transshipped from inland terminal d to port (per day)
q'_d	Containers to be transshipped from port to inland terminal d (per day)
$tt_{i,j}$	Total trip time between nodes i and j (loading, travel, unloading), measured in slots
$\tau_{i,j}$	Pure travel time between nodes i and j (minutes)
$td_{i,j}$	Travel distance between nodes i and j (km)
l	Loading time at port (including internal travel), measured in slots
l'	Unloading time at port (including internal travel), measured in slots
ι	Decoupling time at CRG/inland terminals (including repositioning), measured in slots
ι'	Coupling time at CRG/inland terminals (including repositioning), measured in slots
cap_t	Port truck-handling capacity in slot t (trucks/slot)
cap'_t	Remote gate truck-handling capacity in slot t (trucks/slot)
Q	Target truck arrival rate at the port specified by the operator (trucks/hour)
η	Number of time slots within one hour (here $\eta = 6$ for $\Delta = 10$ minutes)
fc	Daily fixed operating cost of BE truck type k (£/day)
c	Total cost of ownership (TCO) per km for BE truck type k (£/km)
fc'	Daily fixed operating cost of ICE truck type v (£/day)
c'	TCO per km for ICE truck type v (£/km)
wc^{ICE}	Queuing cost of ICE truck per slot at the CRG (£/slot)
wc^{BE}	Queuing cost of BE truck per slot (port or CRG) (£/slot)
pc	Parking cost per truck (or chassis) per slot (£/slot)
e	CO_2 emissions of BE truck type k in queuing per slot (tons/slot)
e'	CO_2 emissions of ICE truck type v in queuing per slot (tons/slot)
ec	Monetary cost of CO_2 emissions (per ton) in queuing state (£/ton)
M	A sufficiently large constant
lc	Unit cost of land per acre (£/acre)
co	Number of chassis that can be stored per acre (chassis/acre)
cu	Daily chassis hiring cost (£/day)
ρ	Unit penalty for late delivery beyond the planning horizon (£/hour)

Table 2 Model decision and derived variables for the integrated truck scheduling formulation

Notation	Definition
Decision variables	
$x_{v,t,d}$	1 if truck v departs from inland terminal d to the CRG in slot t, 0 otherwise
$x'_{v,t,d}$	1 if truck v departs from the CRG to inland terminal d in slot t, 0 otherwise
$y_{k,t}$	1 if truck k departs from the port to the CRG in slot t, 0 otherwise
$y'_{k,t}$	1 if truck k departs from the CRG to the port in slot t, 0 otherwise
$a_{k,t}$	1 if truck k is assigned to a port crane for loading in slot t, 0 otherwise
$a'_{k,t}$	1 if truck k is assigned to a port crane for unloading in slot t, 0 otherwise
$b_{v,t,d}$	1 if truck v from inland terminal d is assigned to the CRG to release a chassis in slot t, 0 otherwise
$b'_{v,t,d}$	1 if truck v starts coupling a chassis in slot t before departing to inland terminal d, 0 otherwise
$b1_{k,t}$	1 if truck k starts coupling a chassis in slot t before departing to the port, 0 otherwise
$b1'_{k,t}$	1 if truck k arriving from the port starts releasing a chassis at the CRG in slot t, 0 otherwise
u_k	1 if BE truck k is used in the planning horizon, 0 otherwise
u'_v	1 if ICE truck v is used in the planning horizon, 0 otherwise
L	Land area rented at the CRG location (acres)
γ	Number of chassis hired per day
Derived variables	
α_t	Queue length of BE trucks at the port in slot t
α'_t	Queue length of BE trucks at the CRG in slot t
θ_t	Queue length of ICE trucks at the CRG in slot t
β_t	Number of BE trucks idle (parked) at the port in slot t
β'_t	Number of BE trucks idle (parked) at the CRG in slot t
λ_t	Number of ICE trucks idle (parked) at the CRG in slot t
cap_t^{BE}	CRG capacity (in trucks per slot) allocated to BE trucks in slot t
cap_t^{ICE}	CRG capacity (in trucks per slot) allocated to ICE trucks in slot t
$dir_{k,t}$	Direction of truck k in slot t (port$\rightarrow$CRG or CRG$\rightarrow$port)
$dir'_{v,t}$	Direction of truck v in slot t (inland terminal$\rightarrow$CRG or CRG$\rightarrow$inland terminal)
δ_t	Number of BE trucks serving at the port (under crane) in slot t
δ_t^{BE}	Number of BE trucks serving at the CRG in slot t
δ_t^{ICE}	Number of ICE trucks serving at the CRG in slot t
π_t	Number of chassis present at the CRG in slot t, excluding queued chassis
ϕ_t	Number of chassis present at the port in slot t

3.2 Mathematical formulation

PHTSP. The objective is to determine the optimal trucks scheduling with minimum aggregated cost. The indices, parameters, and variables are listed in Tables 1 and 2. The MILP model for the PHTSP is formulated at follows:

$$\begin{aligned}\text{Minimize} &\sum_{k\in K}\sum_{t\in T}\left(y_{k,t}\, td_{p,r} + y'_{k,t}\, td_{r,p}\right)\cdot c + \sum_{d\in D}\sum_{v\in V}\sum_{t\in T}\left(x_{v,t,d}\, td_{d,r} + x'_{v,t,d}\, td_{r,d}\right)\cdot c' \\ &+ \sum_{k\in K} u_k \cdot fc + \sum_{v\in V} u'_v \cdot fc' + \sum_{t\in T}(\alpha_t + \alpha'_t)\, wc^{BE} \\ &+ \sum_{t\in T}\theta_t\, wc^{ICE} + \sum_{t\in T}(\beta_t + \beta'_t + \lambda_t)\cdot pc \\ &+ \sum_{t\in T}\theta_t \cdot e' \cdot ec + \sum_{t\in T}(\alpha_t + \alpha'_t)\cdot e \cdot ec + L \cdot lc + \gamma \cdot cu,\end{aligned} \tag{1}$$

The objective function (1) minimizes the total system cost. The first and second terms represent the transportation costs of BE and ICE trucks, respectively, while the third and fourth terms account for their operating costs. The fifth and sixth terms represent the queuing costs incurred by BE and ICE trucks, respectively. The seventh term corresponds to the parking cost associated with idle trucks. The eighth and ninth terms account for the emissions costs generated by BE and ICE trucks during queuing, respectively. Finally, the last two terms represent the land rental cost at the CRG and the chassis hiring cost.

To improve the readability and transparency of the MILP formulation, the constraints are structured into seven functional groups corresponding to the main modeling components: (i) BE truck movement and location constraints, (ii) port service and demand fulfillment constraints, (iii) ICE truck movement and location constraints, (iv) CRG service and queuing constraints, (v) truck utilization constraints, (vi) chassis inventory and requirement constraints, and (vii) variable domain constraints.

3.2.1 BE truck movement and location constraints

The BE truck movement and location constraints (Constraints (2)–(10)) describe the operational movements of BE trucks between the port and the CRG. These constraints ensure that each truck performs no more than one movement within a given time period, satisfies travel-time requirements, maintains movement flow continuity, and departs only from its current location.

$$y_{k,t} + y'_{k,t} \;\le\; 1, \quad \forall k \in K,\; t \in T \tag{2}$$

$$y_{k,t} + \sum_{\substack{t'\in T \\ t+1\le t'\le t+tt_{r,p}-1}} \left(y_{k,t'} + y'_{k,t'}\right) \;\le\; 1, \quad \forall k \in K,\; t \in T, \tag{3}$$

$$y'_{k,t} + \sum_{\substack{t'\in T \\ t+1\le t'\le t+tt_{p,r}-1}} \left(y_{k,t'} + y'_{k,t'}\right) \;\le\; 1, \quad \forall k \in K,\; t \in T, \tag{4}$$

$$\sum_{k\in K}\sum_{t\in T} y_{k,t} = \sum_{v\in V}\sum_{t\in T}\sum_{d\in D} x_{v,t,d}, \tag{5}$$

$$\sum_{k\in K}\sum_{t\in T} y'_{k,t} = \sum_{v\in V}\sum_{t\in T}\sum_{d\in D} x'_{v,t,d}, \tag{6}$$

$$dir_{k,t} = dir_{k,t-1} + y_{k,t-1} - y'_{k,t-1}, \quad \forall k \in K, \ \forall t = 2, \ldots, |T|, \tag{7}$$

$$y_{k,t-1} \leq 1 - dir_{k,t-1}, \quad \forall k \in K, \ \forall t = 2, \ldots, |T|, \tag{8}$$

$$y'_{k,t-1} \leq dir_{k,t-1}, \quad \forall k \in K, \ \forall t = 2, \ldots, |T|, \tag{9}$$

$$y'_{k,t} \leq \sum_{\substack{t' \in T \\ t < t' \leq t + tt_{r,p}}} y_{k,t'}, \quad \forall k \in K, \ t \in T, \tag{10}$$

Constraint (2) ensures that each BE truck performs at most one operation during each time slot, preventing it from departing simultaneously from both the port and the remote gate. Constraint (3) enforces the travel time requirement for trucks departing from the port to the remote gate. If truck k departs at time t ($y_{k,t} = 1$), it remains occupied for the subsequent $tt_{p,r} - 1$ time slots t'. Therefore, it cannot be reassigned to any other departure, either from the port ($y_{k,t'}$) or from the remote gate ($y'_{k,t'}$), until the trip is completed. Constraint (4) applies the same logic to inbound trips from the remote gate to the port. Constraints (5) and (6) represent the flow balance of inbound and outbound activities, respectively. Together, constraints (7)–(9) ensure location consistency over time. Specifically, a truck can depart from a node only if it is present at that node, and its location status is updated dynamically as it travels between the port and the remote gate. Constraint (10) links outbound trips from the remote gate to the corresponding inbound trips from the port. In particular, a truck may return from the remote gate ($y'_{k,t}$) only if it has previously departed from the port ($y_{k,t}$) within the relevant travel time window $tt_{r,p}$, thereby ensuring consistency between outbound and return movements.

3.2.2 Port service and demand constraints

The port service and demand constraints (Constraints (11)–(18)) formulate the loading and unloading operations at the port, enforce crane capacity limitations, quantify truck queue formation, regulate truck arrivals to the port, and ensure that the daily transport demand is satisfied.

$$\delta_t = \sum_{k \in K} \sum_{\substack{t' \in T \\ t' \leq t < t' + l'_p}} a_{k,t'} + \sum_{k \in K} \sum_{\substack{t' \in T \\ t' \leq t < t' + l_p}} a'_{k,t'}, \quad \forall t \in T, \tag{11}$$

$$\delta_t \leq cap_t, \quad \forall t \in T, \tag{12}$$

$$\alpha_t \ \geq \ \alpha_{t-1} + \delta_{t-1} - cap_{t-1}, \quad \forall t = 2, \ldots, |T|, \tag{13}$$

$$a_{k,t} \leq \sum_{\substack{t' \in T \\ t' = t + tt_{r,p} - l'_p}} y_{k,t'} \quad \forall k \in K, \forall t \in T, \tag{14}$$

$$a'_{k,t} \leq \sum_{t' \leq t} y'_{k,t'} \quad \forall k \in K, \forall t \in T, \tag{15}$$

$$\sum_{t=(h-1)s+1}^{hs} \sum_{k \in K} y'_{k,t} \ \leq \ Q \qquad \forall h \in H \tag{16}$$

$$\sum_{k \in K} \sum_{t \in T} y_{k,t} = \sum_{d \in D} q'_d, \tag{17}$$

$$\sum_{k \in K} \sum_{t \in T} y'_{k,t} = \sum_{d \in D} q_d \tag{18}$$

Constraint (11) defines port crane utilization over time, where the right-hand side counts all trucks engaged in loading and unloading operations during time slot t. Constraint (12) imposes the capacity limit of port cranes, ensuring that the number of simultaneously served trucks does not exceed available crane capacity. Constraint (13) quantifies the number of trucks waiting in the port queue at each time period. Constraints (14) and (15) link truck assignment decisions to the initiation of loading and unloading operations, ensuring that crane operations can only begin once a truck has been assigned and has arrived within the feasible time window.

Constraint (16) regulates the number of trucks departing from the remote gate to the port per hour, ensuring alignment with the target arrival rate Q specified by the port operator. Constraints (17) and (18) ensure that total truck trips satisfy daily container demand in both directions between the port and the remote gate.

3.2.3 ICE truck movement and location constraints

The ICE truck movement and location constraints (Constraints (19)–(27)) govern the movements of ICE trucks between inland terminals and the CRG. Similar to the BE truck movement constraints (Constraints (2)–(10)), these constraints ensure travel-time feasibility, maintain location consistency, and guarantee that transport demand is fulfilled.

$$x_{v,t,d} + x'_{v,t,d} \ \leq \ 1, \quad \forall v \in V, \ t \in T \tag{19}$$

$$x_{v,t,d} + \sum_{\substack{t' \in T \\ t+1 \leq t' \leq t+tt_{d,r}-1}} \left(x_{v,t',d} + x'_{v,t',d}\right) \ \leq \ 1, \quad \forall v \in V, \ t \in T, \ d \in D, \tag{20}$$

$$x'_{v,t,d} + \sum_{\substack{t' \in T \\ t+1 \leq t' \leq t+tt_{r,d}-1}} \left(x_{v,t',d} + x'_{v,t',d}\right) \ \leq \ 1, \quad \forall v \in V, \ t \in T, \ d \in D, \tag{21}$$

$$dir'_{v,t} = dir'_{v,t-1} + \sum_{d \in D} x_{v,t-1,d} - \sum_{d \in D} x'_{v,t-1,d}, \quad \forall v \in V, \ \forall t = 2, \ldots, |T|, \tag{22}$$

$$x_{v,t-1,d} \leq 1 - dir'_{v,t-1}, \quad \forall v \in V, \ \forall t = 2, \ldots, |T|, \ d \in D, \tag{23}$$

$$x'_{v,t-1,d} \leq dir'_{v,t-1}, \quad \forall v \in V, \ \forall t = 2, \ldots, |T|, \tag{24}$$

$$x'_{v,t,d} \leq \sum_{\substack{t' \in T \\ t < t' \leq t+tt_{r,d}}} x_{v,t',d}, \quad \forall v \in V, \ t \in T, \ d \in D, \tag{25}$$

$$\sum_{v\in V}\sum_{t\in T} x_{v,t-1,d} = q'_d, \quad \forall d \in D, \tag{26}$$

$$\sum_{v\in V}\sum_{t\in T} x'_{v,t-1,d} = q_d, \quad \forall d \in D, \tag{27}$$

Constraint (19) ensures that each truck v can perform only one operation at any given time; that is, a truck cannot simultaneously depart from the inland terminals and the remote gate within the same time slot. Constraints (20) and (21) ensure that travel time requirements are satisfied for trucks moving between inland terminals and the remote gate in both directions. Constraints (22)–(24) enforce location feasibility by ensuring that trucks depart only from nodes where they are present, with locations updated dynamically. Constraint (25) links outbound trips from the inland terminals to corresponding inbound trips from the remote gate. Specifically, a truck may return from the remote gate ($x'_{v,t,d}$) only if it previously departed from the inland terminal ($x_{v,t,d}$) within the relevant travel time window $tt_{r,d}$, ensuring consistency between outbound and return trips. Constraints (26) and (27) ensure that container demand between inland terminals and the remote gate is fully satisfied.

3.2.4 CRG service constraints

The CRG service constraints (Constraints (28)–(37)) model truck processing operations at the CRG, including service utilization, capacity allocation, queue evolution, and coupling/decoupling operations.

$$\delta_t^{BE} = \sum_{k\in K} \sum_{\substack{t'\in T\\ t'\le t<t'+\iota'}} b1_{k,t'} + \sum_{k\in K} \sum_{\substack{t'\in T\\ t'\le t<t'+\iota}} b1'_{k,t'}, \quad \forall t \in T, \tag{28}$$

$$\delta_t^{ICE} = \sum_{v\in V} \sum_{\substack{t'\in T\\ t'\le t<t'+\iota'}} \sum_{d\in D} b_{v,t',d} + \sum_{v\in V} \sum_{\substack{t'\in T\\ t'\le t<t'+\iota}} \sum_{d\in D} b'_{v,t',d}, \quad \forall t \in T, \tag{29}$$

$$\delta_t^{BE} + \delta_t^{ICE} \le cap'_t, \quad \forall t \in T, \tag{30}$$

$$\alpha'_t \;\ge\; \alpha'_{t-1} + \delta_{t-1}^{BE} - cap_{t-1}^{BE}, \quad \forall t = 2, \ldots, |T|, \tag{31}$$

$$\theta_t \;\ge\; \theta_{t-1} + \delta_{t-1}^{ICE} - cap_{t-1}^{ICE}, \quad \forall t = 2, \ldots, |T|, \tag{32}$$

$$cap_t^{BE} + cap_t^{ICE} \le cap'_t \quad \forall t \in T, \tag{33}$$

$$b_{v,t,d} \le \sum_{\substack{t'\in T\\ t'=t+tt_{d,r}-\iota'}} x_{v,t',d} \quad \forall v \in V, \forall t \in T, \forall d \in D, \tag{34}$$

$$b'_{v,t,d} \le \sum_{t'\le t} x'_{v,t',d} \quad \forall v \in V, \forall t \in T, \forall d \in D, \tag{35}$$

$$b1'_{k,t} \leq \sum_{\substack{t' \in T \\ t'=t+tt_{p,r}-\iota'}} y_{k,t'} \quad \forall k \in K, \forall t \in T, \tag{36}$$

$$b1_{k,t} \leq \sum_{t' \leq t} y'_{k,t'} \quad \forall k \in K, \forall t \in T, \tag{37}$$

Constraints (28) and (29) define CRG service utilization by BE and ICE trucks at each time slot t, respectively. Constraint (30) enforces the CRG capacity limit, ensuring that the number of trucks in service does not exceed available capacity. Constraints (31) and (32) update the number of BE and ICE trucks waiting in the CRG queue, ensuring that queue lengths reflect excess demand beyond available service capacity for each truck type. Constraint (33) links total CRG capacity to its allocation between BE and ICE trucks by ensuring that the sum of type-specific capacities does not exceed the exogenous capacity limit.

Constraints (34)–(37) link truck assignment decisions to the initiation of decoupling and coupling operations at the CRG, ensuring that these activities begin only after trucks have been assigned and have arrived within the feasible time window.

3.2.5 Truck utilization constraints

The truck utilization constraints (Constraints (38)–(42)) link fleet activation variables with truck operations and determine the number of idle trucks waiting at the port and the CRG.

$$\sum_{t \in T} (y_{k,t} + y'_{k,t}) \leq M.u_k, \quad \forall k \in K, \tag{38}$$

$$\sum_{t \in T} \sum_{d \in D} (x_{v,t,d} + x'_{v,t,d}) \leq M.u'_v, \quad \forall v \in V, \tag{39}$$

$$\beta_t \geq \sum_{k \in K} \sum_{\substack{t' \in T \\ t'+l_p \leq t}} a_{k,t'} - \sum_{k \in K} \sum_{\substack{t'' \in T \\ t'' \leq t}} y_{k,t''}, \quad \forall t \in T, \tag{40}$$

$$\beta'_t \geq \sum_{k \in K} \sum_{\substack{t' \in T \\ t'+\iota \leq t}} b1'_{k,t'} - \sum_{k \in K} \sum_{\substack{t'' \in T \\ t'' \leq t}} y'_{k,t''}, \quad \forall t \in T, \tag{41}$$

$$\lambda_t \geq \sum_{v \in V} \sum_{\substack{t' \in T \\ t'+\iota \leq t}} \sum_{d \in D} b_{v,t',d} - \sum_{v \in V} \sum_{\substack{t'' \in T \\ t'' \leq t}} \sum_{d \in D} x'_{v,t'',d}, \quad \forall t \in T, \tag{42}$$

Constraints (38) and (39) link assignment decisions to truck usage variables. Constraint (40) computes the number of idle BE trucks at the port in slot t, while Constraints (41) and (42) compute the number of idle BE and ICE trucks at the CRG, respectively.

3.2.6 Chassis inventory constraints

The chassis inventory constraints (Constraints (43)–(47)) track chassis inventory throughout the system, determine the maximum chassis inventory required at the CRG for estimating the required land area, monitor chassis movements, and calculate the overall chassis requirement.

$$\pi_t = \pi_0 + \sum_{\substack{t' \in T \\ t' \leq t}} (\sum_{k \in K} b1'_{k,t'} + \sum_{v \in V} \sum_{d \in D} b_{v,t',d}) - \sum_{\substack{t'' \in T \\ t'' \leq t}} (\sum_{k \in K} y'_{k,t''} + \sum_{v \in V} \sum_{d \in D} x'_{v,t'',d}), \quad \forall t \in T, \tag{43}$$

$$L \geq \pi_t, \quad \forall t \in T \tag{44}$$

$$\begin{aligned} tr_t = & \sum_{k \in K} \sum_{\substack{t' \in T \\ t' \leq t < t' + tt_{p,r}}} y_{k,t'} + \sum_{k \in K} \sum_{\substack{t' \in T \\ t' \leq t < t' + tt_{r,p}}} y'_{k,t'} \\ & + \sum_{v \in V} \sum_{\substack{t' \in T \\ t' \leq t < t' + tt_{d,r}}} \sum_{d \in D} x_{v,t',d} + \sum_{v \in V} \sum_{\substack{t' \in T \\ t' \leq t' \leq t < t' + tt_{r,d}}} \sum_{d \in D} x'_{v,t',d}, \quad \forall t \in T. \end{aligned} \tag{45}$$

$$\phi_t = \phi_0 + \sum_{k \in K} \sum_{\substack{t' \in T \\ t' + tt_{r,p} \leq t}} y'_{k,t'} - \sum_{k \in K} \sum_{\substack{t'' \in T \\ t'' \leq t}} y_{k,t''}, \quad \forall t \in T. \tag{46}$$

$$\gamma \geq \pi_t + \alpha'_t + \theta_t + tr_t + \phi_t \quad \forall t \in T, \tag{47}$$

Constraint (43) computes the number of chassis present at the CRG at each time slot t by accounting for cumulative arrivals and departures, where π_0 denotes the initial number of chassis at the CRG, assumed to be zero. Constraint (44) then determines L, the maximum number of chassis present at any time, which is used to compute the required land rental area at the CRG. Constraint (45) determines, for each time period, the number of chassis-coupled trucks traveling between the CRG and the port, as well as between inland terminals and the CRG. Constraint (46) computes the number of idle chassis-coupled trucks parked at the port, awaiting new assignments. Constraint (47) specifies the maximum number of chassis required in the system across the CRG, in transit, and at the port.

3.2.7 Variable domain constraints

The variable domain constraints (Constraints (48)–(50)) define the allowable domains of the decision and auxiliary variables, including binary, integer and non-negative continuous variables.

$$\begin{aligned} & x_{v,t,d},\ x'_{v,t,d},\ y_{k,t},\ y'_{k,t},\ a_{k,t},\ a'_{k,t},\ b_{v,t,d},\ b'_{v,t,d},\ b1_{k,t},\ b1'_{k,t},\ dir_{k,t},\ dir'_{v,t},\ u_k,\ u'_v \quad \in \{0, 1\}, \\ & \forall v \in V,\ k \in K,\ d \in D,\ t \in T. \end{aligned} \tag{48}$$

$$\gamma,\ \alpha_t,\ \alpha'_t,\ \theta_t,\ \beta_t,\ \beta'_t,\ \lambda_t,\ \delta_t,\ \delta_t^{BE},\ \delta_t^{ICE},\ cap_t^{BE},\ cap_t^{ICE},\ \pi_t,\ tr_t,\ \phi_t \in \mathbb{Z}_{\geq 0}, \quad \forall t \in T. \tag{49}$$

$$L \geq 0 \tag{50}$$

4 Two-stage adaptive genetic algorithm for PHTSP

Although advanced solution methods, such as Benders decomposition, column generation, and hybrid machine learning-optimization frameworks, have demonstrated strong capabilities in solving large-scale MILP problems, their applicability depends on the mathematical structure and decomposability of the underlying problem. For the proposed PHTSP, truck movements, queue dynamics, and time-dependent handling capacities at the port and CRG are strongly coupled throughout the planning horizon, which makes an effective decomposition strategy challenging without substantially reformulating the original model. Consequently, a tailored TS-AGA is developed to obtain high-quality solutions for large-scale instances while preserving the detailed constraints of the CRG-BET-based port-hinterland system.

The main innovations of the proposed TS-AGA are threefold. First, unlike conventional GA-based truck scheduling approaches that search the complete fleet-sizing and scheduling space simultaneously, the proposed TS-AGA introduces a hierarchical search strategy that decomposes the optimization into fleet sizing and truck scheduling. This substantially reduces the dimensionality of the search space while preserving the interaction between strategic and operational decisions. Second, the chromosome encoding and fitness evaluation are specifically designed for the CRG-BET system, where scheduling feasibility depends on truck availability at required locations rather than individual truck identities, resulting in a more compact search space and improved computational efficiency. Third, adaptive crossover and mutation operators dynamically balance exploration and exploitation to enhance solution diversity and convergence when solving large-scale instances with complex operational constraints.

Accordingly, the TS-AGA operates in two sequential stages. The first stage determines the optimal fleet composition, including the required numbers of BE and ICE trucks. Based on this fleet configuration, the second stage searches for a near-optimal truck schedule that minimizes the total system cost while satisfying all operational constraints. The overall framework of the proposed TS-AGA is presented in Algorithm 1.

4.1 Solution encoding

The chromosome design must align with the specific characteristics of the problem. In this study, a novel multi-layer chromosome structure is introduced to effectively model potential solutions for the truck scheduling problem. The encoding scheme is composed of three vectors: a container index vector, a direction vector, and a inland terminal index vector. All three vectors share the same dimension, equal to the total number of inbound and outbound containers, $q_d + q'_d$. This representation is straightforward to implement and facilitates both presentation and coding, while also accounting for the variation in travel times among different inland terminals. Alternatively, the chromosome could be structured as a cell array that combines all three elements (container index, direction, and inland terminal index) within each entry. Fig. 3 presents an example of the chromosome representation, illustrating the structure of the three vectors. In this example, we assume $q_d = 10$ and $q'_d = 10$. The indices 0 and 1 in the second vector indicate the container direction: from the port to the inland terminals and from the inland terminals to the port, respectively. Furthermore, it is assumed that the system includes three inland terminals.

Algorithm 1 Two-Stage Adaptive Genetic Algorithm (TS-AGA)

Stage 1: Fleet-size search
Require: Instance data; initial AGA parameter bounds; search limits
Ensure: Best truck fleet $(n^*_{\mathrm{ICE}}, n^*_{\mathrm{BE}})$ minimizing total cost
Compute minimum ICE and BE fleet sizes (lower bounds) from travel and operation times
Compute upper bounds on fleet sizes as a function of total container jobs
Randomly initialize a fleet-size composition $(n^{(0)}_{\mathrm{ICE}}, n^{(0)}_{\mathrm{BE}})$ within these bounds
Set outer counter $s \leftarrow 0$ and no-improvement counter $n \leftarrow 0$
while $s < s_{\max}$ **and** $n < n_{\max}$ **do**
  $s \leftarrow s + 1$
  Select large-to-small step factor z_s
  $\Delta n^{(s)}_{\mathrm{ICE}} = \max\big(1, \lfloor z_s\, n^{(s-1)}_{\mathrm{ICE}} \rfloor\big)$, $\Delta n^{(s)}_{\mathrm{BE}} = \max\big(1, \lfloor z_s\, n^{(s-1)}_{\mathrm{BE}} \rfloor\big)$
  Generate candidate fleets around $(n^{(s-1)}_{\mathrm{ICE}}, n^{(s-1)}_{\mathrm{BE}})$:
    $(n_{\mathrm{ICE}}, n_{\mathrm{BE}}) \in \{(n^{(s-1)}_{\mathrm{ICE}}, n^{(s-1)}_{\mathrm{BE}}), (n^{(s-1)}_{\mathrm{ICE}} \pm \Delta n^{(s)}_{\mathrm{ICE}}, n^{(s-1)}_{\mathrm{BE}}), (n^{(s-1)}_{\mathrm{ICE}}, n^{(s-1)}_{\mathrm{BE}} \pm \Delta n^{(s)}_{\mathrm{BE}})\}$
  Project candidates onto $[n^{\min}_{\mathrm{ICE}}, n^{\max}_{\mathrm{ICE}}] \times [n^{\min}_{\mathrm{BE}}, n^{\max}_{\mathrm{BE}}]$
  Initialize AGA parameters for schedule evaluation.
  for each candidate fleet $(n_{\mathrm{ICE}}, n_{\mathrm{BE}})$ **do**
    Fix fleet sizes in the model: $n_{\mathrm{ICE}}, n_{\mathrm{BE}}$
    Run a AGA with small iterations and small population size and evaluate the best schedule cost $C_{\mathrm{fleet}}(n_{\mathrm{ICE}}, n_{\mathrm{BE}})$
    Update the current best fleet and cost if C_{fleet} improves
  end for
  If no fleet candidate improves the current cost, increment n
end while
Stage 2: Schedule optimization
Ensure: Best schedule S^* for the selected fleet
Fix $(n_{\mathrm{ICE}}, n_{\mathrm{BE}}) \leftarrow (n^*_{\mathrm{ICE}}, n^*_{\mathrm{BE}})$ in the model
Generate an initial population P_0 of n_{pop} candidate chromosomes
Decode each chromosome into a schedule S_i
Evaluate each $S_i \in P_0$ with the cost function $f(S_i)$
Set best solution $S^* \leftarrow \arg\min_{S_i \in P_0} f(S_i)$ and best cost $C^* \leftarrow f(S^*)$
Compute initial diversity D_0 and initialize history $H \leftarrow \emptyset$
Initialize adaptive control parameters: mutation rate $p_m^{(0)}$, crossover rate $p_c^{(0)}$
for $it = 1$ to $MaxIter$ **do**
  Crossover:
    Select parent pairs via roulette-wheel sampling
    Apply uniform crossover to the container index vectors with rate $p_c^{(it)}$ to obtain offspring set P_c
  Mutation:
    Select parents via roulette-wheel sampling
    Apply neighbourhood mutation (swap, insertion, reversal) with rate $p_m^{(it)}$ to obtain mutant set P_m
  Decode all offspring and mutants into schedules; evaluate $f(S)$
  Merge populations: $P \leftarrow P \cup P_c \cup P_m$ and retain the best n_{pop} individuals (elitist truncation)
  Update S^* and C^* if an improved solution is found, Update C^{W} and recompute population diversity D_{it}
  Adaptive control:
  Compute improvement rate and stall counter based on C^* and H
  Adapt $(p_c^{(it)}, p_m^{(it)})$ using improvement rate and diversity:
    increase exploration (higher p_m) if diversity is low or stall persists
    increase exploitation (lower p_m) when improvements are frequent and diversity is adequate
  Append C^* to history H
  Stopping rules:
  if maximum function evaluations reached **or** stall exceeds limit **or** best-cost history flattens **then**
    break ▷ Early termination based on adaptive rules
  end if
end for
return S^*, $(n^*_{\mathrm{ICE}}, n^*_{\mathrm{BE}})$, C^*

Container index	8	16	4	15	9	12	17	1	18	10	19	3	7	20	11	13	14	5	2	6
Container direction	1	0	1	0	1	0	0	1	0	1	0	1	1	0	0	0	0	1	1	1
Inland terminal index	3	2	1	2	3	1	2	1	3	3	3	1	2	3	1	1	1	2	1	2

Fig. 3 Chromosome structure

4.2 Solution decoding

Algorithm 2 presents the procedure for interpreting the chromosome structure. This step translates a randomly generated chromosome into a candidate solution, either feasible or infeasible, for the port-hinterland truck scheduling problem. The decoding process proceeds sequentially from left to right. In this example (see Fig. 3), the first element of the first vector is 8, representing the container index, while the corresponding elements of the second and third vectors are 1 and 3, respectively. These values indicate that the container is transported from inland terminal 3 to the port. According to Algorithm 2, the availability status of truck v is checked, and if the truck is available, it is assigned to the container. After pickup and arrival at the remote gate, and once a slot is assigned, the truck leaves the chassis (container 8) at the designated area. Its status, including location and availability time, is then updated. Once the first layer is completed, the container proceeds to the second-layer transshipment. This begins with an availability check for truck k. If truck k is available, the remote gate availability for pickup must be checked before the truck can proceed to the port. Upon arrival at the port, a port crane is assigned based on its availability, and after completing the unloading operation, the status of truck k, including its location and next available time, is updated. If no truck is available at any stage, the container index is added to a waiting list until a suitable truck becomes available. Throughout the procedure, all relevant statistics are recorded. Finally, once no containers remain in the chromosome, the overall cost is calculated.

4.3 Evolutionary phase of TS-AGA

After establishing the chromosome representation and decoding procedure, the evolutionary phase of TS-AGA is applied to improve the solution quality of the port-hinterland truck scheduling problem.

4.3.1 Population generation and fitness assessment

The evolutionary process begins with the generation of an initial population of n_{pop} chromosomes. Each chromosome represents a potential truck scheduling solution and is decoded into a corresponding schedule using the decoding procedure described previously. The fitness of each chromosome is evaluated based on the total cost of the decoded schedule, including penalty terms associated with constraint violations, such as capacity exceedance and operations beyond the planning horizon. Since the objective is cost minimization, chromosomes with lower costs are considered fitter and have a higher probability of being selected for reproduction.

4.3.2 TS-AGA operators

High-quality solutions in the TS-AGA are generated through the iterative application of selection, recombination, and mutation across successive generations.

Algorithm 2 Solution Decoding Algorithm

Require: Chromosome, Cap , Cap', $tt_{i,j}$, $\tau_{i,j}$, and the values of other relevant parameters.
Ensure: Aggregated Cost
1: Initialize states:
    v_state, k_state ▷ truck availability times and locations
    CRG_usage, $port\_usage$
    w, w' ▷ w = list of containers waiting at port or inland terminals, w' = list of containers waiting at CRG
    $idle\_times$ (v, k, containers), $queue\_times$ (v, k)
2: **for** each container j following the sequence in the chromosome's first vector: **do**
3:     **if** w or $w' \neq \emptyset$ **then**
4:         Apply 6-45 steps.
5:     **end if**
6:     **if** container direction = 1 **then**
7:         $j \leftarrow container\_id$
8:         Find the earliest available trucks v at inland terminal
9:         **if** no v available **then**
10:             Add j to w; **continue** to next container index
11:         **end if**
12:         Assign v, record first layer start-time ($x_{v,t,d}$)
13:         Schedule inland terminals → CRG trip and record arrival at CRG
14:         Assign CRG decoupling slot ($b_{v,t,d}$)
15:         Update v state, record truck in queue time (α'_t).
16:         Find available k at CRG
17:         **if** no k available **then**
18:             Add j to w'; **continue** to next container index
19:         **end if**
20:         Assign k and CRG coupling slot ($b1_{k,t}$), record departure time ($y'_{k,t}$) and truck idle times (β'_t)/container idle-time.
21:         Schedule CRG → Port trip and record arrival time at port.
22:         Assign Port crane slot for unloading ($a'_{k,t}$).
23:         Update k state, record truck in queue time (α_t).
24:         Record container completion times.
25:     **else if** container direction = 0 **then**
26:         $j \leftarrow container\_id$
27:         Find the earliest available k at port.
28:         **if** no k available **then**
29:             Add j to w; **continue** to next container index
30:         **end if**
31:         Assign k, record first-layer start-time ($y_{k,t}$)
32:         Assign Port crane slot for loading ($a_{k,t}$).
33:         Schedule Port → CRG trip and record arrival-time
34:         Assign CRG decoupling slot ($b1'_{k,t}$)
35:         Update k state, record truck in queue time (α'_t).
36:         Find the earliest available v at CRG
37:         **if** no v available **then**
38:             Add j to w'; **continue** to next container index
39:         **end if**
40:         Assign v and CRG coupling slot ($b'_{v,t,d}$), record departure time ($x'_{v,t,d}$) and truck idle times (λ_t)/container idle-time
41:         Schedule CRG → inland terminal trip, record arrival time
42:         Update v state
43:         Record container completion times
44:     **end if**
45: **end for**
46: Collect statistics and calculate overall cost

Selection The selection mechanism determines the chromosomes participating in reproduction. In this study, roulette-wheel selection is employed to select parent chromosomes according to their fitness values. After generating new offspring through crossover and mutation, an elitist truncation strategy is applied, where all individuals are ranked according to their fitness values and only the best n_{pop} chromosomes are retained for the next generation.

Crossover operator for the sequencing vector

The crossover operator generates new offspring by combining information from selected parent chromosomes. In this study, uniform crossover is applied to the container index vector, which determines the processing sequence of containers. Two parent chromosomes are selected using roulette-wheel selection, and a binary mask with a length equal to the container index vector is randomly generated. For each offspring, elements are inherited from the first parent when the corresponding mask value is one and from the second parent otherwise. The complementary inheritance rule is applied to generate the second offspring. The associated direction and inland terminal indices are transferred together with their corresponding container elements to maintain chromosome feasibility.

Mutation operators for the sequencing vector

Mutation is introduced to maintain population diversity and reduce the risk of premature convergence. Three neighbourhood-based mutation operators, including swap, insertion, and reversal, are applied to the container index vector of selected chromosomes. Each operator is selected with equal probability. The swap operator exchanges two container positions, the insertion operator relocates one container element to another position, and the reversal operator reverses the order of a selected subsequence. The corresponding direction and inland terminal indices are updated consistently with the modified container sequence.

5 Experimental results and discussions

5.1 Benchmark problem setup

To evaluate the effectiveness of the proposed model, 24 test instances of varying scales were generated based on empirical data collected from multiple sources. These instances were proportionally derived from the real case study in terms of container volumes, inland terminal demand, and facility capacities, thereby ensuring a fair and consistent comparison between the exact optimization approach and the proposed solution algorithm. Table 3 shows the test problems configurations,

5.2 Data collection and empirical analysis

Truck arrival data were obtained following the method described by Mokhtari-Moghadam et al. (2025), using inductive loop detector data collected by National Highways on the primary approach road to the port (National Highways, 2025). However, because the sensor is located upstream of the port and some trucks leave the highway before reaching the port, the recorded truck counts were adjusted by applying a 70% scaling factor, based on expert estimates provided by the port operator. The TTT, defined as the duration between gate entry and port exit is extracted from the port's publicly available dashboard. For this study, the average TTT is considered, with a reported value of 40 min (Transport, 2025).

Table 3 Test instance configurations and scale classification

Scale	Instance	Containers ($q'_d = q'$)	Inland terminal demands					Port capacity (truck/hr)†			CRG capacity (truck/hr)†		
			d_1	d_2	d_3	d_4	d_5	LB	μ	UB	LB	μ	UB
Small	P01	50	20	10	10	5	5	2	3	4	5	6	7
	P02	75	20	27	14	7	7	3	5	6	7	9	10
	P03	100	27	36	19	9	9	4	6	7	8	11	13
	P04	125	33	46	24	11	11	5	7	9	10	13	16
	P05	150	40	55	27	14	14	6	9	11	12	17	19
	P06	200	54	74	38	17	17	7	12	15	16	22	25
	P07	250	68	92	46	22	22	10	14	18	21	28	31
	P08	300	80	110	56	27	27	11	17	22	24	33	37
Medium	P09	350	94	130	64	31	31	13	21	25	30	40	44
	P10	400	108	147	73	36	36	16	24	29	32	41	50
	P11	450	122	166	82	40	40	18	26	32	36	48	55
	P12	500	134	184	92	45	45	19	30	36	40	54	62
	P13	550	148	202	100	50	50	24	35	40	44	58	68
	P14	600	162	220	110	54	54	23	36	43	47	63	74
	P15	650	176	238	118	59	59	28	42	47	52	66	80
	P16	700	190	256	128	63	63	29	44	50	56	70	86
Large	P17	750	203	274	137	68	68	26	44	54	59	84	92
	P18	800	217	293	146	72	72	32	51	58	63	82	99
	P19	850	230	311	155	77	77	30	49	61	67	91	105
	P20	900	244	328	164	82	82	36	57	65	71	94	111
	P21	950	258	346	174	86	86	38	56	68	75	103	117
	P22	1000	273	365	182	90	90	35	61	72	79	105	123
	P23	1050	286	382	192	95	95	43	64	75	85	106	129
	P24	1100	300	400	200	100	100	43	67	79	88	123	136

† LB and UB denote the lower and upper bounds of the discrete uniform distribution used to generate hourly port and CRG capacities, expressed as multiples of μ. The bounds range from $0.57\mu - 1.35\mu$ (port) and $0.70\mu - 1.23\mu$ (CRG)

The service time at the CRG, representing the time required for chassis decoupling and coupling operations, is assumed to be 15 min (Dekker et al., 2013). The same service time is also assumed for the inland terminals. Truck travel times between the inland terminals, the CRG, and the port were obtained from Google Maps under free-flow or normal traffic conditions (Google Maps, 2025) and are presented in Table 4. In addition, the desired hourly truck-handling capacity for external trucks at the port is set at 46 trucks per hour, which represents the target capacity required to ensure smooth and continuous operations, including loading and unloading activities, while maintaining efficient truck flows on port access roads (Port-Operator, 2025). However, the actual truck-handling capacity of yard cranes varies throughout the day due to operational priorities, which typically favor seaside operations, as well as potential operational disruptions. Therefore, this study assumes that the available truck-handling capacity changes hourly. Based on an assumed 70% utilization of port-yard capacity for hinterland truck operations, the hourly truck-handling capacity is defined within the range presented in Table 3. This approach captures periods of reduced handling availability while ensuring that external truck demand can be accommodated over the planning horizon. The same approach is applied to the CRG truck-handling capacity to prevent congestion from simply shifting from the port to the CRG, despite its location outside the city boundary.

The travel costs of BE and ICE trucks are based on the TCO, expressed in £/km, with values of £0.945/km and £0.775/km, respectively, adopted from Wang et al. (2024). The TCO includes both capital expenditure (CAPEX) and operating expenditure (OPEX). For BE trucks, the TCO corresponds to Scenario 2, which assumes a plug-in grant of £25,000. The OPEX includes only fuel (or electricity), maintenance, insurance, and CO_2 charges, while driver-related costs are excluded. Therefore, in this study, the labour cost for operating both BE and ICE trucks is estimated separately based on the hourly wage of a truck driver (SalaryExpert, 2025). After including overhead costs (Department for Transport, 2025), the total labor cost is assumed to be £20.29 per hour.

The waiting costs of BE and ICE trucks while queuing at the port/CRG gate are estimated based on energy consumption during the waiting period, assuming that trucks remain in a stationary idle condition throughout the queuing process. For ICE trucks, this includes diesel fuel consumption during idling with the engine running, whereas for BE trucks it includes auxiliary electricity consumption required to maintain vehicle systems while stationary. In both cases, maintenance and vehicle wear costs incurred during the waiting period are included. Driver costs during queuing are calculated separately, as described above, and are included in the truck operating cost regardless of whether the vehicle is traveling, waiting in the queue, or receiving service.

Heavy-duty diesel engines typically consume approximately 2.42 liters of fuel per hour while idling (Radius, 2025). Assuming a diesel price of £1.46 per liter (Wang et al., 2024), the idling fuel cost is approximately £3.53 per hour. Adding an estimated maintenance and engine wear cost of £2.00 per hour (Waste360, 2017) results in a total ICE truck queuing cost of approximately £5.53 per hour, excluding driver costs. For BE trucks, under mild ambient temperatures and without refrigeration, a BE truck consumes approximately 2 kWh of electricity per hour while stationary (Cenex, 2023). Using an electricity price of £0.177 per kWh (Wang et al., 2024), the electricity cost is estimated at approximately £0.35 per hour. Assuming that the maintenance and vehicle wear costs of a BE truck are 67% of those of an ICE truck (Wang et al., 2024), the corresponding maintenance and wear cost is estimated at £1.30 per hour. Therefore, the total queuing cost of a BE truck is estimated to be approximately £1.65 per hour, excluding driver costs.

To estimate CO_2 emissions during queuing, trucks waiting at the port/CRG gate are assumed to operate under idling conditions, representing heavy congestion where vehicles

Table 4 Cost, emission, and operational parameters used in the mathematical model

Symbol	Description	Value	Source
cw^{BE}	BE truck queuing cost (powered on, excl. driver)	£1.65/h	Cenex (2023); Wang et al. (2024)
cw^{ICE}	ICE truck queuing cost (engine on, excl. driver)	£5.53/h	Radius (2025); Waste360 (2017)
e	CO_2 emissions of queued BE truck	279 gCO_2/h	Mokhtari-Moghadam et al. (2025)
e'	CO_2 emissions of queued ICE truck	4118 gCO_2/h	Barlow and Cairns (2020)
ce	Cost of CO_2 emissions	£49.41/t CO_2	Uk Desnz (2025)
cu	Chassis hiring price	£70/week	Port-Operator (2025)
co	Chassis occupancy per acre	35 units/acre	Port-Operator (2025)
c	Total cost of ownership per km (BE truck)	£0.945/km	Wang et al. (2024)
c'	Total cost of ownership per km (ICE truck)	£0.775/km	Wang et al. (2024)
$td_{d,r}$	Distance inland terminal-remote gate	45–148 km	Google Maps (2025)
$\tau_{d,r}$	Travel time inland terminal-remote gate	40–120 min	Google Maps (2025)
$td_{p,r}$	Distance port-remote gate	38 km	Google Maps (2025)
$\tau_{p,r}$	Travel time port-remote gate	40 min	Google Maps (2025)
fc, fc'	Daily truck operating cost (24-hour, three-shift operation including full driver and overhead costs)	£486.96/day	SalaryExpert (2025)
pc	Parking cost per truck per hour	£1.9/h	Ashford International (2026)
lc	Annual land lease cost per acre (local area)	£60,173/year	Port-Operator (2025)
ρ	Penalty cost of late delivery	£200/h	Based on operating and delay costs

remain stationary. The idling CO_2 emission rate for an ICE truck is 68.64 g CO_2/min (Barlow and Cairns, 2020), corresponding to 4118 g CO_2/h. For BE trucks, CO_2 emissions during queuing are estimated based on the corresponding electricity consumption reported by Mokhtari-Moghadam et al. (2025). Table 4 summarizes the data sources and parameter values used in this study. The late delivery penalty is set at £200/h, estimated from the hourly operating cost of a truck, including vehicle and driver-related costs. This value represents the combined direct and indirect economic impacts associated with delivery delays. It is worth noting that, in the discrete-time formulation presented in Section 3, the hourly queuing, parking, and emission cost parameters listed in Table 4 are converted to per-slot values based on a 10-minute time slot and applied to the slot-based queuing and idle-time variables in the objective function.

5.3 Computational result and analysis

5.3.1 Experimental design and computational setup

In this section, the performance of the proposed TS-AGA for solving the PHTSP is evaluated against both an exact MILP approach and a metaheuristic benchmark. The exact approach relies on Gurobi 13.0.1 to solve the MILP formulation of the problem, while the metaheuristic benchmark is a two-stage simulated annealing (TS-SA) algorithm. The test bed consists of 24 instances of varying size, covering small, medium, and large-scale problems.

For the MILP benchmark, TS-AGA is compared with the best incumbent solution returned by Gurobi within a time limit of 10,800 s (3 h). This comparison is reported for the small- and medium-scale instances, where Gurobi is able to identify feasible incumbents and valid lower bounds. To ensure a fair comparison of search effort, TS-AGA is run under a set of adaptive stopping criteria: the maximum number of function evaluations (NFE) is capped at 500, and the algorithm monitors search progress over a rolling window of the most recent 500 evaluations. The search terminates when the relative improvement in the best objective value within this window falls below 1%, which prevents excessive computation once convergence is detected.

To further assess the effectiveness of the proposed search strategy, the TS-AGA is compared with a TS-SA algorithm across all 24 test instances. The TS-SA is developed by extending the conventional simulated annealing (SA) algorithm with the same two-stage optimization framework adopted by TS-AGA, in which the first stage determines the fleet composition and the second stage optimizes the truck scheduling decisions. This ensures that both algorithms operate under an identical problem decomposition, allowing differences in performance to be attributed solely to their search mechanisms. The comparison is particularly important for medium- and large-scale instances, where Gurobi is unable to obtain a feasible solution (incumbent) for the MILP model within the prescribed time limit and can only provide a lower bound (LB).

Furthermore, both TS-AGA and TS-SA employ the same maximum NFE and relative improvement threshold as their stopping criteria. Unlike TS-SA, which is a single-solution local search algorithm that evaluates one candidate solution per iteration, TS-AGA is a population-based metaheuristic that evaluates multiple candidate solutions in each generation through crossover and mutation operators. Therefore, using NFE as the primary stopping criterion provides both algorithms with an identical computational budget in terms of objective function evaluations, enabling a fair and unbiased comparison of their search performance.

The TS-AGA and TS-SA algorithms were implemented in MATLAB R2024a, while the MILP model was implemented in Python and solved using Gurobi 13.0.1. All computational experiments were performed on a personal computer equipped with an Intel Core i5 processor running at 3.10 GHz and 16 GB of RAM.

5.3.2 Computational results and discussion on small- and medium-scale instances

Table 5 presents a summary of the computational results obtained by the TS-AGA and the exact MILP method solved using Gurobi for the small- and medium-scale test problems (P1-P16). The first column indicates the scale of the test instances, while the second column lists the individual instances. The third to sixth columns report the Gurobi results, including the best feasible objective value (incumbent), LB, computational time, and MILP optimality gap, respectively. Columns 7–10 present the TS-AGA results, including the best-found feasible solution, the mean objective value over five independent runs, the coefficient of variation (CV), calculated as the standard deviation divided by the mean objective value, and the average computational time, respectively. The final two columns report the relative deviations of the TS-AGA best solution from the Gurobi incumbent and lower bound, respectively, as defined in the footnote.

For the small-scale instances, Gurobi was unable to obtain the optimal solution within the prescribed time limit for all instances, resulting in optimality gaps ranging from 0.06% to 5.39%. In contrast, TS-AGA demonstrated strong performance across all small-scale instances (P1-P8), outperforming Gurobi's best feasible solution in half of the instances

Table 5 Performance comparison between the MILP model solved by Gurobi and the TS-AGA on small- and medium-scale test instances

Scale	Instance	MILP (Gurobi)				TS-AGA				TS-AGA vs. MILP	
		Incumbent	LB	CPU (s)	Gap (%)	Best	Mean (5-run)	CV (%)	Mean CPU (s)	Gap to Inc. (%)[a]	Gap to LB (%)[b]
Small	P1	18,190	18,178	10800	0.06	18,289	18,385	0.70	15	0.54	0.61
	P2	27,951	27,836	10800	0.41	28,018	28,285	0.83	33	0.24	0.66
	P3	38,180	37,091	10800	2.85	37,280	37,532	0.64	34	−2.36	0.51
	P4	49,011	46,365	10800	5.39	47,549	47,707	0.23	47	−2.98	2.55
	P5	56,453	55,813	10800	1.13	56,061	56,243	0.34	65	−0.70	0.44
	P6	74,840	73,848	10800	1.33	74,935	75,068	0.16	113	0.13	1.47
	P7	94,486	92,452	10800	2.15	93,141	93,555	0.44	175	−1.42	0.75
	P8	112,259	111,079	10800	1.05	112,433	112,732	0.22	231	0.16	1.22
Medium	P9	130,852	129,939	10800	0.70	130,044	130,376	0.23	269	−0.62	0.08
	P10	151,487	149,298	10800	1.45	151,058	151,985	0.40	275	−0.28	1.18
	P11	168,013	166,005	10800	1.20	167,438	168,513	0.40	403	−0.34	0.86
	P12	–	185,765	10800	–	185,975	186,161	0.10	531	–	0.11
	P13	–	204,151	10800	–	205,311	205,654	0.13	637	–	0.57
	P14	–	223,056	10800	–	226,263	226,630	0.13	676	–	1.44
	P15	–	241,107	10800	–	244,393	245,193	0.23	795	–	1.36
	P16	–	258,287	10800	–	262,852	263,540	0.23	958	–	1.77

[a]Gap to Inc. (%) is calculated as $(\text{Best}_{\text{TS-AGA}} - \text{Incumbent}_{\text{MILP}})/\text{Incumbent}_{\text{MILP}} \times 100$; negative values indicate better TS-AGA solutions. [b]Gap to LB (%) is calculated similarly using the MILP lower bound

(P3, P4, P5, and P7). Furthermore, the TS-AGA best solutions remained within 2.55% of the Gurobi lower bound for all instances.

For the medium-scale test instances, Gurobi was able to find feasible solutions only for the first three instances (P9-P11), achieving optimality gaps ranging from 0.70% to 1.45% within the three-hour time limit. In contrast, TS-AGA produced comparable or better solutions for these instances within 403 s when compared with Gurobi's best feasible solutions. For the remaining instances (P12-P16), Gurobi was only able to provide lower bounds within the imposed time limit, whereas TS-AGA successfully obtained feasible solutions for all instances within 958 s. Moreover, the relative deviation of the TS-AGA best solutions from the corresponding lower bounds remained below 1.77%. As indicated by the CV (%) values, TS-AGA demonstrates robust and consistent performance across all small- and medium-scale test instances, with the coefficient of variation remaining below 1% in every case.

The proposed TS-AGA is compared with TS-SA on both small- and medium-scale test instances, and the computational results are summarized in Table 6. The first and second columns indicate the instance scale and test instances, respectively, while columns 3-7 and 8-12 present the results of TS-AGA and TS-SA, respectively, including the best-found solution, the mean objective value over five independent runs, standard deviation (SD), average computational time, and CV. The final column reports the percentage improvement of the TS-AGA best-found solution over the TS-SA best-found solution.

Comparing the results for the small-scale instances shows that both algorithms perform well in solving all P1-P8 instances in terms of solution quality and computational efficiency, benefiting from the common two-stage problem decomposition into fleet composition optimization and truck scheduling optimization. The best-found solutions obtained by TS-AGA are consistently superior to those produced by TS-SA, except for the first instance (P1). The values in the last column indicate that, although TS-SA achieved a slightly better solution for P1, TS-AGA outperformed TS-SA in the remaining seven instances, with improvements ranging from 0.46% to 1.70%. Similarly, TS-AGA achieved lower average objective values in seven of the eight test instances. In terms of computational time, however, TS-SA was consistently faster than TS-AGA across all small-scale instances. Both algorithms demonstrated robust performance, with the CV remaining below 1% in every case. Nevertheless, TS-SA exhibited lower CV values than TS-AGA in five of the eight instances, indicating slightly greater solution consistency for these relatively small problems.

As the problem size increases to the medium-scale instances, TS-AGA consistently outperforms TS-SA in terms of solution quality while requiring almost the same computational time. Furthermore, TS-AGA demonstrates superior robustness, as evidenced by its lower SD and CV across all medium-scale instances. This enhanced stability can be attributed to its population-based search mechanism combined with adaptive operators, which provide a better balance between exploration and exploitation of the search space. In contrast, TS-SA exhibits noticeably greater variability in solution quality, as reflected by its higher SD and CV values, indicating that its robustness deteriorates as the problem size increases.

5.3.3 Computational results and discussion on large-scale instances

Table 7 compares the performance of TS-AGA and TS-SA for large-scale test instances, with the MILP lower bound provided as a reference to evaluate solution quality. For these instances, Gurobi failed to obtain feasible solutions within the prescribed time limit. In contrast, both TS-AGA and TS-SA successfully obtained high-quality solutions, with average deviations of 1.22% and 1.50%, respectively, from the MILP lower bound. Both algorithms completed within approximately 15–35 min per instance, exhibiting comparable computational times

Table 6 Performance comparison between TS-AGA and TS-SA on small- and medium-scale test instances

Scale	Instance	TS-AGA					TS-SA					TS-AGA advantage (%)[a]
		Best	Mean	SD	Mean CPU (s)	CV (%)	Best	Mean	SD	Mean CPU (s)	CV (%)	
Small	P1	18,289	18,385	128	15	0.70	18,255	18,310	63	11	0.35	−0.18
	P2	28,018	28,285	234	33	0.83	28,502	28,514	13	17	0.05	1.70
	P3	37,280	37,532	241	34	0.64	37,465	37,837	319	28	0.84	0.49
	P4	47,549	47,707	109	47	0.23	47,770	48,207	301	12	0.62	0.46
	P5	56,061	56,243	192	65	0.34	56,566	56,634	90	15	0.16	0.89
	P6	74,935	75,068	118	113	0.16	76,070	76,116	53	25	0.07	1.49
	P7	93,141	93,555	412	175	0.44	93,840	94,252	318	33	0.34	0.74
	P8	112,433	112,732	248	231	0.22	113,027	113,623	626	169	0.55	0.53
Medium	P9	130,044	130,376	299	269	0.23	130,510	130,903	437	177	0.33	0.36
	P10	151,058	151,985	615	275	0.40	151,666	152,897	1,235	234	0.81	0.40
	P11	167,438	168,513	678	403	0.40	167,964	169,148	1,338	287	0.79	0.31
	P12	185,975	186,161	194	531	0.10	186,135	186,889	836	497	0.45	0.09
	P13	205,311	205,654	261	637	0.13	206,039	206,712	687	643	0.33	0.35
	P14	226,263	226,630	293	676	0.13	226,880	228,214	886	738	0.39	0.27
	P15	244,393	245,193	557	795	0.23	245,662	246,489	820	830	0.33	0.52
	P16	262,852	263,540	604	958	0.23	263,754	265,043	1,174	936	0.44	0.34

[a] TS-AGA advantage (%) is calculated as $(\text{Best}_{\text{TS-SA}} - \text{Best}_{\text{TS-AGA}})/\text{Best}_{\text{TS-SA}} \times 100$; positive values indicate better TS-AGA solutions

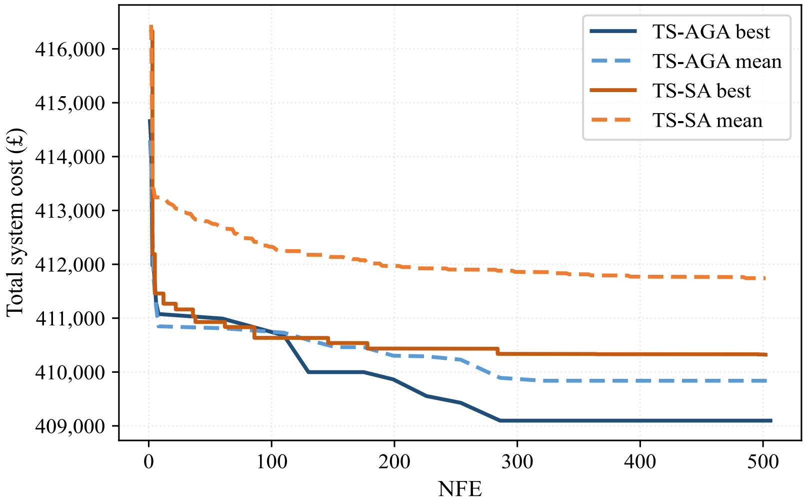

Fig. 4 Convergence comparison of TS-AGA and TS-SA for test instance P24

while consistently producing high-quality solutions. A comparison between TS-AGA and TS-SA shows that TS-AGA consistently outperformed TS-SA by achieving lower total system costs across all large-scale instances (P17-P24), yielding an average cost reduction of 0.29%. Furthermore, the solutions obtained by TS-AGA were more robust, as evidenced by their lower SD and CV. This improved robustness can be attributed to the population-based search strategy and adaptive mechanisms incorporated into TS-AGA.

Fig. 4 illustrates the convergence behaviour of TS-AGA and TS-SA for test instance P24, presenting the best-found and average objective values obtained over five independent runs of each algorithm. As observed, both algorithms achieve a substantial reduction in total cost during the first stage, which evaluates different fleet-size combinations and identifies the fleet configuration that minimizes the total system cost. For the best-found solutions, the first stage of TS-SA determines a fleet consisting of 175 ICE trucks and 130 BE trucks, while TS-AGA identifies a nearly identical configuration comprising 176 ICE trucks and 131 BE trucks. Subsequently, both algorithms utilize their allocated NFE budgets in the second stage to further improve solution quality based on the fleet configuration identified in the first stage.

It is important to note that the convergence curves in Fig. 4 combine the cost reductions achieved in both stages to provide a comprehensive representation of the overall algorithm performance. Therefore, the initial sharp decrease in total system cost shown in the figure results primarily from the fleet-size optimization performed in the first stage, while the subsequent improvements reflect the solution refinement process in the second stage.

Comparing the convergence behaviour of the two algorithms, TS-SA achieves a rapid cost reduction during the initial iterations, but subsequent improvements are marginal, converging to a best-found solution of £410,322 and an average solution value of £411,741. In contrast, TS-AGA exhibits only modest improvement during the early iterations of the second stage; however, after approximately 130 NFEs it continues to reduce the total cost and converges at around 300 NFEs, achieving a best-found total system cost of £409,097 and an average solution value of £409,838. This corresponds to an improvement of approximately 0.3% in the total daily cost relative to TS-SA, as reported in Table 7.

Table 7 Performance comparison between TS-AGA and TS-SA on large-scale test instances

Scale	Instance	MILP (Gurobi) LB	TS-AGA					TS-SA					TS-AGA advantage (%)[a]
			Best	Mean	SD	Mean CPU (s)	CV (%)	Best	Mean	SD	Mean CPU (s)	CV (%)	
Large	P17	278,375	280,985	281,606	549	933	0.19	282,264	283,270	855	1,106	0.30	0.45
	P18	297,506	301,392	302,299	750	974	0.25	302,110	303,393	1,259	1,180	0.41	0.24
	P19	316,405	322,407	322,958	669	1,121	0.21	323,444	324,524	828	1,274	0.26	0.32
	P20	334,845	337,652	338,337	590	1,337	0.17	338,715	339,594	1,105	1,388	0.33	0.31
	P21	353,764	358,188	359,135	625	1,589	0.17	359,405	360,905	1,132	1,485	0.31	0.34
	P22	372,954	377,161	377,820	551	1,558	0.15	378,091	379,161	949	1,571	0.25	0.25
	P23	389,101	395,936	396,781	893	2,060	0.23	396,299	398,860	1,782	1,727	0.45	0.09
	P24	406,031	409,097	409,838	457	1,949	0.11	410,322	411,741	1,108	1,914	0.27	0.30

[a] TS-AGA advantage (%) is calculated as $(\text{Best}_{\text{TS-SA}} - \text{Best}_{\text{TS-AGA}})/\text{Best}_{\text{TS-SA}} \times 100$; positive values indicate better TS-AGA solutions

Although the improvement in daily cost may appear modest, such savings can accumulate to become significant over long-term continuous operations. It is important to note that both algorithms are implemented within the same two-stage optimization framework, with an identical fleet size determination procedure in the first stage. Therefore, this comparison provides a fair assessment of the convergence characteristics and solution refinement capability of the proposed TS-AGA relative to TS-SA under the same problem decomposition. The results indicate that the adaptive search mechanism of TS-AGA is effective in further improving solution quality after the initial fleet size selection.

In the real-world case (P24), the best solution found by TS-AGA yields a total daily cost of £409,097, comprising travel cost, truck operating cost, waiting and parking cost, queuing CO_2 emission cost, and chassis leasing and land rental cost. The proportion of each cost component is illustrated in Fig. 5. As shown, truck travel cost accounts for the largest share of total cost, amounting to £254,772 (approximately 62.3%). This finding underscores that route optimization and distance reduction are the primary levers for reducing the cost of road-based freight transport. For long-haul movements, decision makers could also consider alternative freight transport modes that exploit economies of scale to achieve further cost reductions. The driver-related operating costs (BE and ICE operating costs combined) amount to £149,496.72, representing approximately 36.5% of total cost, indicating that truck and labor management constitute the second most important cost driver.

The remaining cost components, including queuing, parking, queue-related emissions, and chassis leasing and land rental, together account for approximately 1.2% of total cost. Although daily truck queuing and idling costs are minimized and represent only a small share of the total, their cumulative impact over prolonged operations can be substantial. Savings achieved through reducing queuing and idling can therefore be reinvested to improve overall system performance. It is notable that, as discussed earlier in Section 4, the travel cost is based on the total cost of truck ownership in £/km, which includes CO_2 emissions released during transportation but excludes driver-related costs.

From a practical perspective, this cost decomposition helps managers identify which cost elements can be influenced by network design and dispatching decisions (travel distance and time) versus those governed by contractual and regulatory constraints (wages, rental agreements, and carbon price), and thus where optimization effort and policy interventions should be prioritized.

Figures 6 and 7 depict the comparison between available and utilized truck capacity per hour at the port and CRG, respectively, throughout the planning horizon of test instance P24. The Fig. 6 shows that, in the first hour, BE trucks operate close to the port's hourly capacity when loading container and dispatching it to the CRG. During the second and third hours, some capacity remains unused because other trucks are scheduled to load/unload and move to or from the CRG at the start of the planning horizon. From the fourth hour onward, truck flows follow a smoother pattern, mostly ranging from approximately 40 to 60 trucks per hour, while port capacity fluctuates between roughly 40 and 80 trucks per hour. This gap indicates that capacity constraints are respected and gate congestion is avoided throughout the horizon; extending the planning horizon would likely preserve this balanced pattern of flows between the port and the CRG, indicating that the proposed planning approach enables high utilization without overloading the gate, thereby reducing queuing, improving service reliability, and avoiding the need for short-term capacity expansions or overtime staffing at the port.

A similar observation holds for the CRG in Fig. 7, where during the first hour only a small fraction of the CRG's capacity is used, as a limited number of trucks arrive from the port and inland terminals to decouple their chassis. From the second hour onward, coupling and

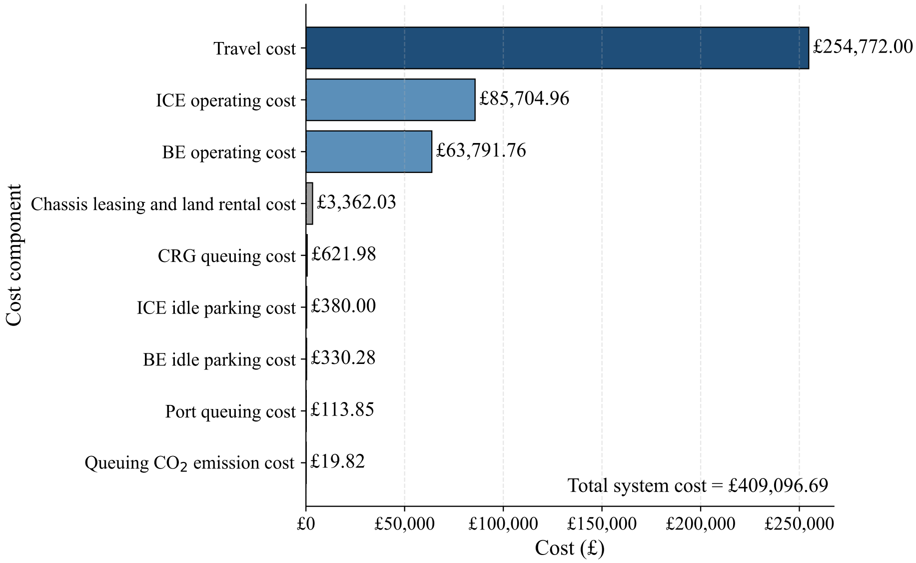

Fig. 5 Breakdown of daily cost components for the best TS-AGA solution to test instance P24

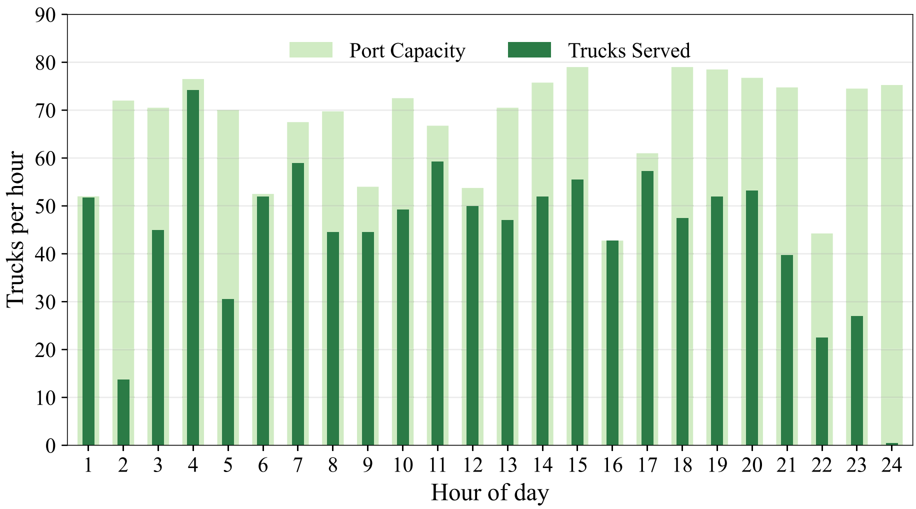

Fig. 6 Hourly port capacity and trucks served for test instance P24

decoupling operations proceed more steadily across the planning horizon, with trucks served remaining consistently below the available gate capacity, thereby maintaining adherence to the CRG's capacity limits. For operators, this implies that the integrated dispatching and fleet management policy produced by the model can be used to schedule truck arrivals within realistic capacity envelopes at both ends of the corridor, supporting stable yard operations and predictable turnaround times. Extending the planning horizon would likely preserve this balanced pattern of flows between the port and the CRG, which is critical for long-

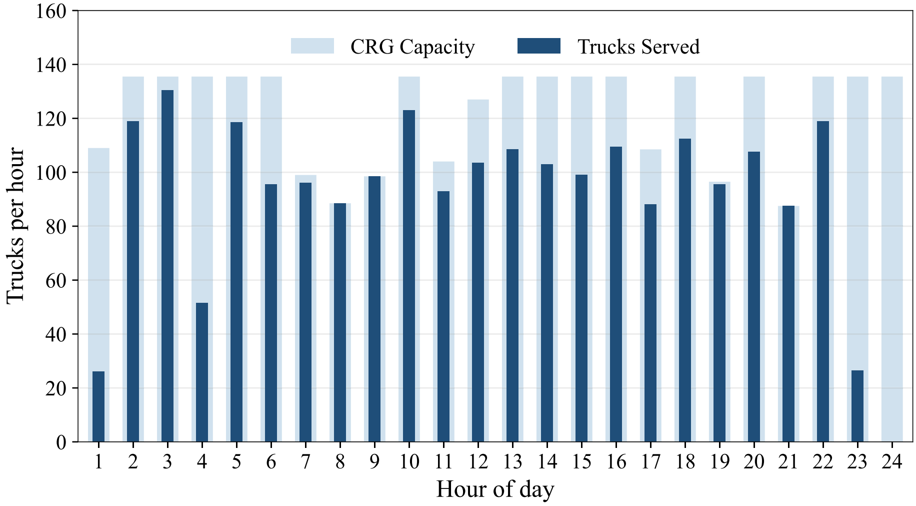

Fig. 7 Hourly CRG capacity and trucks served for test instance P24

term coordination between the port authority, CRG operator, and haulage companies when negotiating service levels and planning infrastructure investments.

The truck utilization metrics for the last test instance are illustrated in Fig. 8, which compares the operating and idle/queue time proportions of ICE and BE trucks. ICE trucks spend 93.1% of their time in operation and 6.9% in idle/queue states, whereas BE trucks spend 88.7 and 11.3%, respectively, indicating slightly higher idle and queue times for the BE fleet under the given scheduling scenario. This high fleet utilization rate highlights the importance of joint scheduling and coordination among port-hinterland stakeholders. By accounting for variations in port and CRG capacity, such coordination can minimize truck non-operational time and reduce the associated costs.

Figure 9 presents the number of trucks in the queue at both the port and the CRG over 10-minute intervals. At the port (blue line), a substantial queue forms at the very beginning of the planning horizon, with more than 90 trucks waiting, but it quickly dissipates and remains negligible for most subsequent intervals. At the CRG (orange line), a large queue builds up shortly after operations start, reaching more than 120 trucks at its peak before gradually declining. Beyond this initial transient, CRG queue lengths fluctuate at much lower levels, with occasional peaks below about 40 trucks and many intervals with no waiting trucks at all. Overall, the trajectories indicate that queuing is concentrated in a short initial period, while for the majority of the horizon both port and CRG queues are small or zero.

As illustrated, the proposed joint scheduling approach can absorb the initial surge in truck arrivals and subsequently stabilize operations without persistent congestion. The consistently low queue levels thereafter suggest that, with an extended planning horizon, continuous gate-capacity expansion may not be necessary. This finding provides reassurance to port and CRG operators that coordinated, optimized schedules can keep truck turnaround times under control and maintain reliable service throughout operations.

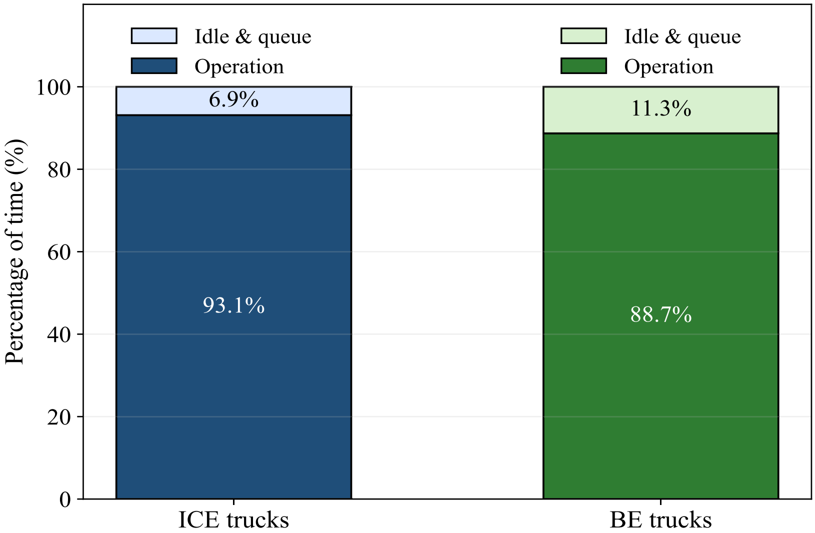

Fig. 8 Comparison of ICE and BE truck utilization profiles based on operating and idle/queue periods for test instance P24

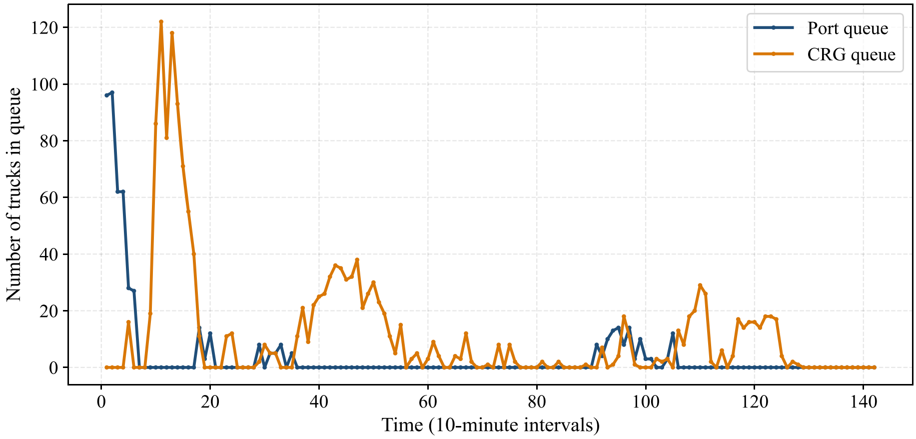

Fig. 9 Port and CRG queue length profiles for test instance P24

5.4 Stakeholder collaboration analysis

This section evaluates the impact of a collaborative scheduling strategy by comparing it with a non-collaborative baseline scenario. In the baseline case, ICE trucks arrive at the CRG according to hourly patterns similar to those observed at the port, without information sharing between the port authority, CRG operator, and trucking companies. In contrast, the collaborative scenario assumes that stakeholders share operational information and follow the optimized schedules generated by the proposed framework.

Figure 10 illustrates the average hourly ICE truck arrival rate at the port over one week in October 2024. The detailed breakdown of system costs under the collaborative scheduling strategy, compared with the non-collaborative baseline scenario, is presented in Table 8. As

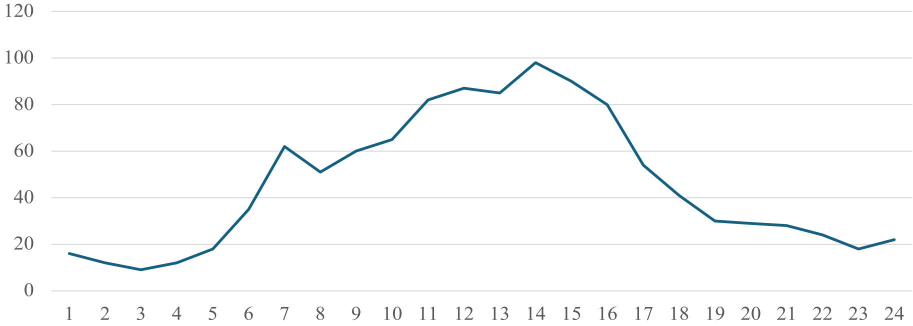

Fig. 10 Average weekly truck arrivals at the port in October 2024

shown in Table 8 and Fig. 11, the collaborative scheduling strategy reduces the total system cost by approximately 13.6% compared with the non-collaborative baseline.

For a terminal operating at the scale of Instance P24, this translates into a daily saving of about £64,000, which can accumulate to several million pounds over a typical year of operations and can be reinvested in overall port-hinterland system improvements. This cost reduction is driven by synchronizing long-haul ICE truck arrivals with short-haul battery-electric truck operations and better aligning truck movements with the available handling capacities at the port and CRG, thereby smoothing demand at the gates and reducing non-productive time. The percentage changes reported in Fig. 11 are calculated using the following expression:

$$\text{Percentage change} = \frac{\text{Cost component}_{\text{collaboration}} - \text{Cost component}_{\text{non-collaboration}}}{\text{Cost component}_{\text{non-collaboration}}} \times 100. \tag{51}$$

where negative values indicate cost reductions achieved by the collaborative scheduling strategy, whereas positive values indicate cost increases compared with the non-collaborative scenario.

The analysis of the cost components shows that the collaborative scheduling strategy substantially reduces ICE truck idle time at the CRG, resulting in an approximately 94% reduction in the associated costs. Consequently, long-haul trucks spend significantly less time waiting in queues or parked idle, improving fleet utilization and enabling hauliers to complete more trips with the same fleet. Synchronizing truck movements with available system capacity also decreases BE truck idle parking costs by 69.2%. Furthermore, the improved scheduling strategy reduces the number of chassis required in the system, leading to reductions of 44.5% in both chassis leasing and land rental costs; this demonstrates how better coordination can defer or avoid capital-intensive investments in CRG equipment and space.

The CRG queuing cost and the CO_2 emission cost associated with truck queuing are also reduced by 31.5 and 28.2%, respectively, highlighting that collaboration not only lowers operating expenditure but also supports environmental and sustainability targets by cutting unnecessary emissions from queued trucks. In contrast, the port queuing cost for BE trucks increases from £39.03 to £113.85, representing an absolute increase of £74.82; however, its contribution to the overall system cost remains negligible and can be interpreted as a minor side-effect of prioritizing the reduction of ICE queuing at the CRG. The largest cost saving is achieved in ICE truck operating costs, which decrease by approximately £53,565 (38.5%)

Table 8 Cost comparison between the collaborative and non-collaborative approaches for the real-world case study (Instance P24)

Cost component	No collaboration (baseline) Cost (£)	Collaboration approach Cost (£)
Travel cost	254,772.00	254,772.00
ICE operating cost	139,270.56	85,704.96
BE operating cost	65,118.82	63,791.76
CRG queuing cost	907.59	621.98
Port queuing cost	39.03	113.85
ICE idle parking cost	6,207.45	380.00
BE idle parking cost	1,071.98	330.28
Queuing CO_2 emissions cost	27.62	19.82
Chassis leasing and land rental cost	6,052.71	3,362.03
Total system cost	473,467.77	409,096.69

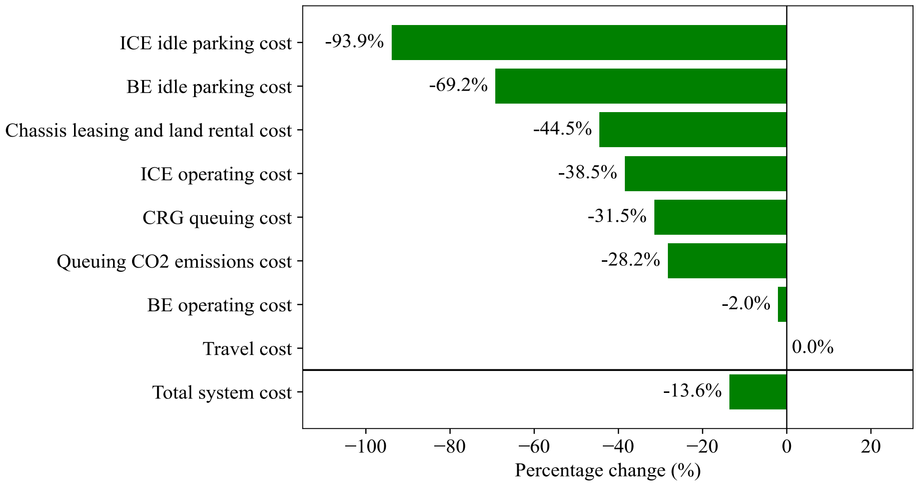

Fig. 11 Tornado plot of collaboration impacts on cost components (excluding port queuing cost)

under the collaborative scheduling strategy, while BE truck operating costs are also reduced by 2%. Overall, these results provide clear evidence that information sharing and coordinated scheduling between the port, CRG, and haulage operators can deliver substantial economic and environmental benefits, and they offer a quantitative basis for designing incentive schemes or contractual arrangements that encourage stakeholders to adopt collaborative planning practices.

5.5 Sensitivity analysis on traveling time

The travel time of long-haul ICE trucks can fluctuate due to factors such as traffic conditions and weather disruptions. To investigate the impact of this variability, it is assumed that the travel time between inland terminals and the CRG ($\tau_{i,j}$) is subject to random disturbances. In each scenario, the uncertain travel times ($\tilde{\tau}_{i,j}$) are sampled from a uniform distribution within a predefined range, reflecting realistic variations derived from Google Maps. Since the baseline travel times used in the model (as described previously) represent free-flow conditions, the uncertainty ranges are defined to capture potential congestion-related delays.

This sensitivity analysis is conducted using the real-world case study P24 to evaluate the robustness and performance of the proposed TS-AGA. The best solutions obtained from five independent runs are presented in Table 9. It is noteworthy that, although travel time increases, the travel distance ($td_{i,j}$) remains unchanged. Because travel cost is calculated on the basis of distance rather than time, this cost component is unaffected, as shown in Table 9. However, the increase in travel time is reflected in the operating costs. Fig. 12 illustrates the results for the baseline and three sensitivity scenarios; travel cost is excluded for clarity because it remains identical across the baseline and all sensitivity scenarios.

Overall, congestion-related delays experienced by long-haul ICE trucks result in an increase in the total system cost, as shown in Table 9, compared with the baseline. The total cost under the three scenarios increases proportionally with the level of travel-time uncertainty, by approximately 1.3%, 2.7%, and 3.7%, respectively. From Fig. 12, it can be observed that longer travel times for long-haul ICE trucks raise their operating costs, primarily because a larger ICE fleet is required to satisfy demand. In contrast, the BE truck operating cost exhibits a slight overall reduction under the first and second scenarios, followed by an increase under the third scenario due to the additional BE trucks required. Specifically, the ICE fleet sizes for the baseline and the three sensitivity scenarios are 176, 187, 200, and 200 trucks, respectively, whereas the corresponding BE fleet sizes are 131, 130, 127, and 136 trucks, respectively. These figures show that, as congestion worsens, the system responds by deploying more ICE trucks and adjusting the BE fleet, which in turn reshapes queuing and idle-time patterns at the CRG and port.

Under Scenario 1, congestion-related delays modestly increase ICE travel times, but the system absorbs these disruptions by adding ICE capacity and slightly reducing the BE fleet. Although the ICE truck queuing cost at the CRG decreases by 19% compared with the baseline, the ICE truck idle parking cost at the CRG increases substantially (by approximately 31%). This increase is mainly attributed to the larger ICE truck fleet required, which results in more ICE trucks waiting for container exchange with BE trucks, whose fleet size is reduced for short-haul operations. In contrast, the queuing costs of BE trucks at the port and CRG increase slightly by 10% and 3%, respectively, while their idle parking cost decreases by approximately 9%, indicating better utilization of the remaining BE fleet. The CO_2 emission cost associated with queuing ICE trucks at the CRG decreases, whereas the corresponding cost for BE trucks increases marginally due to longer queue duration. Furthermore, the chassis leasing cost increases by 3%, mainly due to the longer travel time of ICE trucks. The land rental cost for chassis accommodation at the CRG also increases by 21% compared with the baseline, reflecting the additional space requirements associated with the extended gate operation. Finally, the system incurs an additional £300 penalty cost due to late container deliveries beyond the planning horizon.

Under Scenario 2, increased congestion-related delays for long-haul ICE trucks necessitate the deployment of a larger ICE fleet, resulting in an approximately 14% increase in ICE truck operating costs. Consequently, the costs associated with ICE truck queuing, idle parking, and CO_2 emissions increase significantly by 64%, 77%, and 64%, respectively. Conversely, BE truck operating costs decrease due to the reduced fleet size, and their queuing cost at the CRG decreases by 29%. However, the BE truck queuing cost at the port increases by a similar percentage, resulting in only a marginal change in the associated queuing CO_2 emission cost. The idle parking cost of BE trucks decreases substantially (by 34%), primarily due to the smaller fleet size and the resulting higher utilization of BE trucks in port-CRG shuttle

Table 9 Sensitivity analysis of ICE truck travel time under different scenarios (£)

Cost component	Baseline ($\tau_{i,j}$)	Scenario 1 ($\tilde{\tau}_{i,j} \sim U[\tau_{i,j}, 1.1\tau_{i,j}]$)	Scenario 2 ($\tilde{\tau}_{i,j} \sim U[\tau_{i,j}, 1.2\tau_{i,j}]$)	Scenario 3 ($\tilde{\tau}_{i,j} \sim U[\tau_{i,j}, 1.3\tau_{i,j}]$)
Travel cost	254,772.00	254,772.00	254,772.00	254,772.00
ICE operating cost	85,704.96	91,061.52	97,392.00	97,392.00
BE operating cost	63,791.76	63,304.80	61,843.92	66,226.56
CRG queuing cost (ICE)	481.11	389.87	790.79	459.91
CRG queuing cost (BE)	140.87	144.73	100.62	165.12
Port queuing cost (BE)	113.85	124.88	148.31	146.93
ICE idle parking cost	380.00	496.53	672.28	385.70
BE idle parking cost	330.28	300.20	216.92	447.13
Queuing CO_2 emission cost (ICE)	17.70	14.34	29.10	16.92
Queuing CO_2 emission cost (BE)	2.12	2.25	2.07	2.60
Chassis hiring cost	3,070.00	3,170.00	3,270.00	3,360.00
Land rental cost	292.03	353.27	353.27	376.82
Late delivery penalty	0.00	300.00	633.33	466.67
Total system cost	409,096.69	414,434.38	420,224.61	424,218.37

Cost values are expressed in pounds

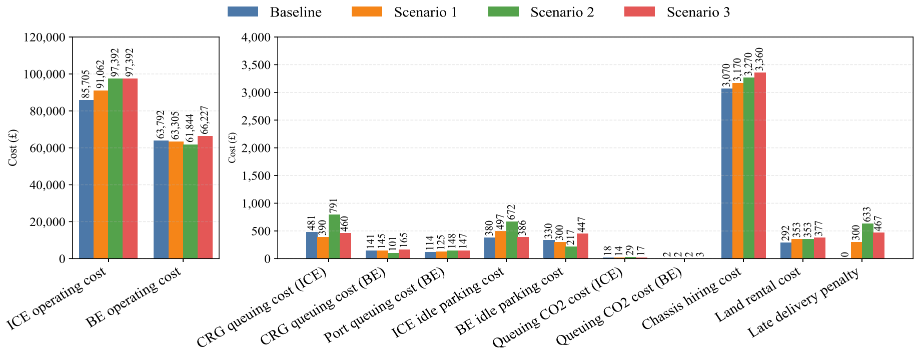

Fig. 12 Illustration of the sensitivity analysis on traveling time of long-haul ICE trucks

operations. Conversely, the chassis leasing cost increases by 7%, mainly due to the longer travel time of ICE trucks. Furthermore, the land rental cost increases by 21%, and late deliveries beyond the planning horizon incur an additional cost of £633.33 to the logistics system.

Under the worst-case scenario, the required ICE truck fleet size remains the same as in Scenario 2 (200 vehicles), representing an increase of 24 trucks compared with the baseline. In contrast, the BE truck fleet size increases to 136 vehicles. Consequently, the operating costs of the ICE and BE fleets increase by approximately 14% and 4%, respectively, relative to the baseline. The larger BE fleet reduces the waiting time of ICE trucks at the CRG for chassis exchange, thereby lowering the associated idle parking cost. However, it increases the idle parking cost of BE trucks. The queuing cost of ICE trucks at the CRG decreases by 4% compared with the baseline, leading to a corresponding reduction in CO_2 emission cost. Conversely, the queuing cost of BE trucks increases because they compete for limited port and CRG resources, resulting in higher CO_2 emission costs. Chassis hiring costs also increase, primarily due to longer congestion-related delays for ICE trucks and the additional land rental cost at the CRG. Finally, although the cost of late container delivery beyond the planning horizon is £467, it is lower than in Scenario 2 because of the larger BE fleet employed.

Overall, this sensitivity analysis shows how congestion on the road network propagates into fleet sizing, utilization, and environmental performance at the CRG and port. Increasing uncertainty in long-haul ICE arrival times forces operators to deploy more vehicles and accept higher queuing, idle-time, and emission costs. However, even under the worst-case scenario considered here, the total economic impact is limited to about 3.7% relative to the baseline. This demonstrates that the proposed TS-AGA framework, when combined with active collaboration and coordination among logistics stakeholders, is robust to plausible levels of congestion and can contain the resulting negative externalities within a relatively narrow band of system-wide cost increases.

5.6 Managerial insights

The computational results provide actionable implications for port authorities, CRG operators, trucking companies, and transport planners. The key insights are as follows:

(1) Establish collaborative scheduling and information-sharing arrangements: The comparison between the collaborative and non-collaborative scenarios shows that coordinated

scheduling reduces total system cost by 13.6% in the real-world instance. This reduction is achieved by synchronizing long-haul ICE truck arrivals with short-haul BE truck operations and aligning truck movements with the time-varying capacities of the port and CRG. Therefore, port authorities, CRG operators, and hauliers should establish mechanisms for sharing expected truck arrival times, gate capacities, container availability, and operational disruptions. In practice, this coordination could be supported through shared digital platforms, advance appointment systems, and jointly agreed operating schedules.

(2) Use differentiated fleet roles rather than a one-size-fits-all fleet strategy: The results support a complementary deployment strategy in which BE trucks are assigned primarily to short-distance shuttle operations between the port and CRG, while ICE trucks undertake longer hinterland movements. This allocation exploits the operational suitability of BE trucks for predictable, repetitive short-haul trips while retaining ICE trucks for movements affected by longer distances and uncertain road travel times. For trucking companies, the implication is that fleet electrification should be accompanied by careful task allocation, rather than simply replacing ICE trucks with BE trucks on all routes.

(3) Prioritize the reduction of travel and operating costs: According to the results travel cost is the largest component of total system cost, accounting for approximately 62.3% in Instance P24, while combined ICE and BE operating costs represent a further 36.5%. Managers should therefore prioritize measures that reduce unnecessary travel distance and improve vehicle productivity, such as route optimization, backhaul matching, improved dispatching, and reduced empty movements. In addition, where technically feasible and permitted by regulation, autonomous truck-platooning technology could help reduce driver-related operating costs. Under such a configuration, a lead truck is operated by a driver, while following trucks travel in a coordinated formation and may require fewer onboard drivers, depending on the applicable automation level and regulatory framework (Lee et al., 2024; Slowik and Sharpe, 2018; Xue et al., 2026). Although queuing and parking costs constitute a comparatively small proportion of daily total cost, reducing them remains important because their cumulative cost, associated emissions, and adverse effects on service reliability can become substantial over prolonged operations.

(4) Coordinate fleet sizing with chassis and yard-capacity decisions: The results show that collaborative planning reduces chassis leasing and land rental costs by 44.5%, demonstrating that fleet scheduling decisions directly affect equipment and space requirements. Operators should therefore determine truck fleet size, chassis availability, and CRG storage capacity jointly rather than independently. This integrated approach can reduce unnecessary chassis inventories and defer costly investments in additional storage space or parking areas.

(5) Incorporate travel-time uncertainty into operational planning: The sensitivity analysis indicates that longer and more uncertain ICE truck travel times increase total system cost by 1.3–3.7%, mainly through higher ICE fleet requirements, operating costs, chassis requirements, and late-delivery penalties. Managers should consequently incorporate road-congestion information, predicted travel times, and contingency capacity into daily planning. The results also indicate that increasing the BE fleet can partly compensate for severe ICE travel disruptions, although this may increase BE idle time and operating costs; hence, contingency fleet decisions should balance resilience against resource costs.

(6) Support decarbonization through electrified short-haul operations: Deploying BE trucks for repetitive short-haul movements between the port and CRG can reduce local emissions and support port-city decarbonization objectives. The results show that coordination can reduce queuing-related CO_2 emission costs by reducing unnecessary truck waiting time.

(7) Plan infrastructure and operational resources jointly: Effective planning of port and CRG resources, including gate-handling capacity, chassis availability, land requirements, and parking space, is essential for efficient system operation. The results demonstrate that time-varying capacities at both facilities should be explicitly considered when developing truck schedules, as ignoring such variation can shift congestion from one facility to another. Joint planning of these resources with fleet deployment and appointment schedules can reduce queuing, avoid unnecessary chassis and land-rental costs, and improve the reliability of port-hinterland operations.
(8) Use the proposed framework as a rolling-horizon decision-support tool: The TS-AGA framework can support operational decisions on truck assignment, departure timing, fleet sizing, and capacity utilization for large-scale port-hinterland systems. Rather than being used solely for long-term planning, the framework could be applied in a rolling-horizon setting in which schedules are periodically updated as new information on traffic conditions, port and CRG capacities, and truck arrivals becomes available. This would enable stakeholders to respond proactively to disruptions while maintaining coordination across the port-CRG-hinterland network.

6 Conclusion

Growing port throughput and long-haul truck movements have intensified congestion and environmental challenges in port-hinterland systems, particularly within port cities. This study develops a sustainability-aware optimization framework for CRG-BET-based port-hinterland truck scheduling, addressing an important gap in existing research. A MILP model coupled with a customized evolutionary algorithm, TS-AGA, is developed to optimize coordinated ICE and BE truck operations while considering time-varying resource availability and operational constraints. The main findings are summarized as follows:

(1) Coordinated scheduling of ICE and BE trucks improves the synchronization between long-haul and short-haul operations by aligning truck movements with available port and CRG capacities, thereby reducing congestion, waiting times, and idle times while enhancing fleet utilization and overall system efficiency.
(2) The proposed framework reduces total logistics system costs, including transportation, waiting, idling, infrastructure-related, and emission costs, while improving the utilization of available port and CRG resources.
(3) Sensitivity analysis demonstrates the robustness of the proposed scheduling framework under long-haul travel-time uncertainty and highlights the need for resilient scheduling strategies under variable operating conditions.
(4) The integration of CRG and BE truck operations, supported by optimized scheduling decisions, provides a practical and scalable approach for improving port-hinterland connectivity, particularly in road-dominated freight networks.

Overall, this study provides actionable insights for port authorities, logistics operators, and policymakers regarding the planning and operation of CRG-based logistics systems supported by BE truck operations. The proposed framework can contribute to reducing congestion, lowering emissions, and improving the efficiency of port-city freight transport.

Although this study incorporates key operational factors relevant to the implementation of the CRG-BET-based port-hinterland truck scheduling, several limitations remain. First, truck repositioning decisions at inland terminals are not considered, as the current research focuses on coordination between long-haul ICE and short-haul BE truck operations within port, CRG, and inland terminals. Incorporating repositioning strategies and associated operational costs would significantly increase the complexity of the optimization problem and represents an important direction for future research. Second, the CO_2 emission parameter used in this study is based on a single grid-mix emission factor. In practice, electricity generation sources vary throughout the day, resulting in time-dependent emission intensities. Furthermore, ICE and BE trucks are assumed to be homogeneous within their respective fleets, with identical operational characteristics and energy consumption rates for each operating state, while travel speeds are assumed to be constant. Future research could incorporate dynamic electricity emission factors and heterogeneous truck fleets to improve the realism of the model. Finally, although the proposed TS-AGA achieves high-quality solutions for small- to large-scale real-world cases, there remains scope for further improving its computational efficiency and scalability. Future research may explore alternative solution strategies, including advanced metaheuristic frameworks, hybrid optimization approaches, and problem-specific decomposition techniques tailored to the temporal coupling characteristics of the port-hinterland truck scheduling problem.

Funding This work was supported by the Liverpool John Moores University (LJMU) Freeport and Net Zero Transport Thematic Doctoral Pathways (FTDP) PhD Scholarship and the Development of AI-Based Digital Platform and Service to Enhance Efficiency and Safety for Ships and PORTs (AI-PASSPORT) project (Grant No. 10126404).

Declarations

Conflict of interest The authors declare that they have no conflict of interest.

References

Afiatno, B. E., Joyoutomo, K. D., & Mukti, K. E. (2025). Model of intermodal competition: A case study in East Java. *Cleaner Logistics and Supply Chain, 17*, Article 100267.

Azab, A., Karam, A., & Eltawil, A. (2020). A simulation-based optimization approach for external trucks appointment scheduling in container terminals. *International Journal of Modelling and Simulation, 40*(5), 321–338.

Ashford International Truckstop. (2026). *Our Tariffs*. https://www.ashfordtruckstop.co.uk/our-tariffs/. Accessed: 2026-06-23.

Bagheri, M., Abbasi, H., Yaghoubi, S., Pishvaee, M. S., & Fallahi, M. (2025). Optimizing dry port locations: A comparative analysis of deterministic, stochastic, and robust models. *Transportation Research Record, 2679*(2), 1922–1940.

Barlow, T., & Cairns, O. (2020). *Idling Action Research - Review of Emissions Data*. Project Report PPR987. TRL Limited. Prepared for: City of London, Project reference ISTAQ001-012, Version 3, Quality approved by Ebony Kaye and Charlie Harding.

Benedecti, R. C., Silva, V. M., & Durski, & Alves da Costa, Gustavo Adolfo. (2024). Integrated simulation of an inland container terminal and waterway service for enhancing the maritime supply chain connectivity between Joinville and Itapoá Port. *Latin American Transport Studies,2*, Article 100019.

Bouchery, Y., Woxenius, J., & Fransoo, J. C. (2020). Identifying the market areas of port-centric logistics and hinterland intermodal transportation. *European Journal of Operational Research, 285*(2), 599–611.

Caballini, C., Gracia, M. D., Mar-Ortiz, J., & Sacone, S. (2020). A combined data mining – optimization approach to manage trucks operations in container terminals with the use of a TAS: Application to an Italian and a Mexican port. *Transportation Research Part E: Logistics and Transportation Review, 142*, Article 102054.

Cenex. 2023. *Deep dive analysis 4: Energy by usage*. Tech. rept. Battery Electric Truck Trial (BETT). Accessed: 2026-04-30.

da Silva, M., Flores, R., Agostino, I. R., & Sousa, & Frazzon, Enzo Morosini. (2023). Integration of machine learning and simulation for dynamic rescheduling in truck appointment systems. *Simulation Modelling Practice and Theory,125*, Article 102747.

Dekker, R., van der Heide, S., van Asperen, E., & Ypsilantis, P. (2013). A chassis exchange terminal to reduce truck congestion at container terminals. *Flexible Services and Manufacturing Journal, 25*(4), 528–542.

Department for Transport. (2025). Overview of the Road Freight Sector: 2024.

Dong, B., Christiansen, M., Fagerholt, K., & Chandra, S. (2020). Design of a sustainable maritime multi-modal distribution network – case study from automotive logistics. *Transportation Research Part E: Logistics and Transportation Review, 143*, Article 102086.

Facchini, F., Digiesi, S., & Mossa, G. (2020). Optimal dry port configuration for container terminals: A non-linear model for sustainable decision making. *International Journal of Production Economics, 219*, 164–178.

Aregall, G., Marta, B., & Rickard, & Monios, Jason. (2018). A global review of the hinterland dimension of green port strategies. *Transportation Research Part D: Transport and Environment,59*, 23–34.

Google Maps. (2025). *Distance between [Location A] and [Location B]*. https://www.google.com/maps. Accessed: February 28.

Guan, C., Liu, R., & (Rachel). (2009). Container terminal gate appointment system optimization. *Maritime Economics & Logistics,11*(4), 378–398.

Guo, T., Liu, P., Wang, C., Xie, J., Du, J., & Lim, M. K. (2023). Toward sustainable port-hinterland transportation: A holistic approach to design modal shift policy mixes. *Transportation Research Part A: Policy and Practice, 174*, Article 103746.

Huynh, N.N., Walton, C., & Michael. (2005). Methodologies for reducing truck turn time at marine container terminals. University of Texas at Austin, Center for Transportation Research. SWUTC/05/167830-1 Tech. rept.

Irawan, C. A., Salhi, S., Jones, D., Dai, J., & Liu, M. J. (2024). A dry port hub-and-spoke network design: An optimization model, solution method, and application. *Computers & Operations Research, 167*, Article 106646.

Kurtuluş, E. (2022). Optimizing inland container logistics through dry ports: A two-stage stochastic mixed-integer programming approach considering volume discounts and consolidation in rail transport. *Computers & Industrial Engineering, 174*, Article 108768.

Lee, C., Dalmeijer, K., Hentenryck, V., & Pascal, & Zhang, Peibo. (2024). Optimizing autonomous transfer hub networks: Quantifying the potential impact of self-driving trucks. *EURO Journal on Transportation and Logistics,13*, Article 100141.

Lättilä, L., Henttu, V., & Hilmola, & Olli-Pekka. (2013). Hinterland operations of sea ports do matter: Dry port usage effects on transportation costs and CO2 emissions. *Transportation Research Part E: Logistics and Transportation Review,55*, 23–42.

Mokhtari-Moghadam, A., Nguyen, T.T., Li, H., Carr, S., Yazdani, D., Yang, Z., & Wang, J. (2025). Sustainable port-city connectivity using remote gates and battery-electric truck operations. SSRN. https://doi.org/10.2139/ssrn.7282658

National Highways. (2025). *Webtris - National Highways*. Accessed: 2025-01-29.

Notteboom, T. E., & Rodrigue, J.-P. (2005). Port regionalization: Towards a new phase in port development. *Maritime Policy & Management, 32*(3), 297–313.

Phan, M.-H., & Kim, K. H. (2015). Negotiating truck arrival times among trucking companies and a container terminal. *Transportation Research Part E: Logistics and Transportation Review, 75*, 132–144.

Port-operator. (2025). Price of Hiring a Chassis Personal communication.

Raad, N. G., Rajendran, S., & Salimi, S. (2022). A novel three-stage fuzzy GIS-MCDA approach to the dry port site selection problem: A case study of Shahid Rajaei Port in Iran. *Computers & Industrial Engineering, 168*, Article 108112.

Radius. (2025). *On Average, How Much Fuel is Wasted by Idling?* Accessed: 2026-04-30.

Rodrigue, J.-P., & Notteboom, T. (2009). The terminalization of supply chains: Reassessing the role of terminals in port/hinterland logistical relationships. *Maritime Policy & Management, 36*(2), 165–183.

Rodrigue, J.-P., Debrie, J., Fremont, A., & Gouvernal, E. (2010). Functions and actors of inland ports: European and North American dynamics. *Journal of Transport Geography*, **18**(4), 519–529. Special Issue on Comparative North American and European gateway logistics.

Roso, V. (2007). Evaluation of the dry port concept from an environmental perspective: A note. *Transportation Research Part D: Transport and Environment, 12*(7), 523–527.
Roso, V., Woxenius, J., & Lumsden, K. (2009). The dry port concept: Connecting container seaports with the hinterland. *Journal of Transport Geography, 17*(5), 338–345.
SalaryExpert. (2025). Truck driver salary in Liverpool, United Kingdom. Accessed: 28 September 2025.
Schulte, F., Lalla-Ruiz, E., González-Ramírez, R. G., & Voß, S. (2017). Reducing port-related empty truck emissions: A mathematical approach for truck appointments with collaboration. *Transportation Research Part E: Logistics and Transportation Review, 105*, 195–212.
Sciomachen, A., & Stecca, G. (2023). Forwarding containers to dry ports in congested logistic networks. *Transportation Research Interdisciplinary Perspectives, 20*, Article 100846.
Slowik, Peter, & Sharpe, Ben. 2018. *Automation and the Long-Haul Trucking Industry*. https://theicct.org/wp-content/uploads/2021/06/Automation_long-haul_WorkingPaper-06_20180328.pdf. Working Paper.
Transport, M. (2025). Liverpool turnaround times fall as Peel Ports improves road-haulage efficiency.
Tsao, Y.-C., & Thuy, L. V. (2018). Seaport- dry port network design considering multimodal transport and carbon emissions. *Journal of Cleaner Production, 199*, 481–492.
UIC, & UIRR. (2024). *2024 Report on Combined Transport in Europe*. Accessed: 2025-10-16.
UK DESNZ. (2025). *UK ETS: Carbon price for use in civil penalties, 2026*. Published 28 November 2025. Accessed: 6 July 2026.
UNCTAD. (1982). *Multimodal transport and containerisation*. Geneva: United Nations Conference on Trade and Development. TD/B/C.4/238/Supplement 1, Part Five: Container and Depots.
van Asperen, E., Borgman, B., & Dekker, R. (2013). Evaluating impact of truck announcements on container stacking efficiency. *Flexible Services and Manufacturing Journal, 25*(4), 543–556.
Veenstra, A., Zuidwijk, R., & van Asperen, E. (2012). The extended gate concept for container terminals: Expanding the notion of dry ports. *Maritime Economics & Logistics, 14*(1), 14–32.
Wang, Z., Acha, S., Bird, M., Sunny, N., Stettler, M. E. J., Wu, B., & Shah, N. (2024). A total cost of ownership analysis of zero emission powertrain solutions for the heavy goods vehicle sector. *Journal of Cleaner Production, 434*, Article 139910.
Waste360. (2017). Trucks: The hidden costs of idling
Wiegmans, B., Witte, P., & Roso, V. (2020). Directional inland port development: Powerful strategies for inland ports beyond the inside-out/outside-in dichotomy. *Research in Transportation Business & Management*, **35**, 100415. Modal shift and logistics integration in intermodal transport networks' in Research in Transportation, Business and Management.
Xue, Z., Peng, W., Zhang, J., & Chen, R. (2026). Two-echelon optimization framework for semi-autonomous truck platooning in container drayage. *Computers & Operations Research, 188*, Article 107343.
Zhao, W., & Goodchild, A. V. (2010). The impact of truck arrival information on container terminal rehandling. *Transportation Research Part E: Logistics and Transportation Review, 46*(3), 327–343.
Zhen, L., Lv, W., Tan, Z., & Dong, B. (2022). Container transportation scheduling between Port Yards and the Hinterland in Yunfeng. *INFORMS Journal on Applied Analytics, 52*(3), 250–266.
Zhuge, D., Wang, S., & Zhen, L. (2024). Shipping emission control area optimization considering carbon emission reduction. *Operations Research, 72*(4), 1333–1351.